The importance of *in situ* crystallisation and loss of interstitial melt during formation of the Kærven Syenite Complex, Kangerlussuaq, East Greenland

PAUL MARTIN HOLM & NIELS-OLE PRÆGEL

Holm, P.M. & Prægel, N-O. 2019. The importance of *in situ* crystallisation and loss of interstitial melt during formation of the Kærven Syenite Complex, Kangerlussuaq, East Greenland. © 2019 by Bulletin of the Geological Society of Denmark, Vol. 67, pp. 107–146, ISSN 2245-7070. (www.2dgf.dk/publikationer/bulletin). https://doi.org/10.37570/bgsd-2019-67-07

Received 19 September 2018
Accepted in revised form
11 July 2019
Published online
24 October 2019

Two supplementary
data files

The Kærven Syenite Complex (KSC) is one of the oldest felsic intrusions in the Tertiary East Greenland province. Here we update our previous description of the KSC and supply a greatly expanded and comprehensive geochemical dataset. New data allow us to present a more detailed petrogenetic model for the evolution of the KSC and to investigate the geochemical characteristics of igneous cumulates subjected to loss and, occasionally, replacement of residual liquid. The KSC comprises eleven mappable units that generally young westwards. Rock types range from quartz syenite to quartz alkali feldspar syenite and alkali feldspar granite. Individual intrusive units are relatively narrow and steep-sided and are collectively suggested to represent a ring dyke complex. Basement gneiss and gabbro host rocks have locally contaminated the oldest quartz syenite KSC unit, but most of the main part of the complex escaped significant influence from host rocks. A late suite of E–W to NE–SW striking peralkaline dykes of trachytic to phonolitic compositions intrude the KSC.

Compositions of the KSC rocks span a considerable range in SiO_2, 59–73 wt%. Concentrations of several elements vary widely for a given SiO_2 (especially at $SiO_2 < 66$ wt%), and variation diagrams do not suggest a single model for the evolution of the units of the complex. A cumulative origin is envisaged for several KSC units. Geochemical modelling suggests that KSC magmas were derived from more than one primary magma, and that the complex evolved through a four-stage process: fractional crystallisation in precursory magma chambers was followed by final emplacement of each unit, establishment of a crystal/melt mush, expulsion of part of the residual melt and, finally, crystallisation of the remaining melt. Trace element disequilibria between alkali feldspar and host rocks in two closely associated quartz alkali feldspar syenite units indicate that highly evolved residual melt was replaced by a less evolved melt phase. Modelling of potential parent melt compositions to the Kærven magmas suggests an origin not in the Iceland plume asthenosphere, but rather in a moderately enriched source, possibly in the continental lithosphere.

The course of melt evolution by fractional crystallisation is indicated to have taken place in magma chambers at depth, and repeated rise of magma into the upper crustal magma chambers and crystallisation there formed the KSC. Based on our survey of published geochemical data, the inferred parental magmas seem to have few equivalents in the North Atlantic Igneous Province and may have been generated mainly from melting of enriched dry lithospheric mantle of possibly Archaean age.

Keywords: Crystal–liquid separation; *in situ* crystallisation; cumulates; syenite; granite; North Atlantic Igneous Province; ring dyke complex; trace elements.

Paul Martin Holm [paulmh@ign.ku.dk], Department of Geosciences and Natural Resource Management, University of Copenhagen, Øster Voldgade 10, DK-1350 Copenhagen, Denmark. Niels-Ole Prægel [nop@kb.dk], Copenhagen University Library, Nørre Allé 49, DK-2200 Copenhagen, Denmark.

Silicic igneous rocks make up a significant part of the upper continental crust (e.g. Wedepohl 1995; Rudnick & Gao 2003). Their formation has been suggested to be caused by direct melting of existing crustal rocks, by magmatic differentiation of mantle-derived mafic melts, or by some combination of these processes, including crustal contamination of mafic magmas (e.g. Petford *et al*. 2000; Bachmann & Huber 2016). Because of the highly viscous nature of silicic melts, crystal settling is highly unlikely to explain their differentiation, and crystal–liquid separation must take place by liquid convection (e.g. Sparks *et al*. 1984; Lee & Morton 2015). Unlike mafic plutonic rocks, the petrographic identification of cumulates has proved difficult for

felsic plutons (e.g. Deering & Bachmann 2010), and the geochemical relationship between rhyolites and granite plutons has remained ambiguous (Lundstrom & Glazner 2016). In this contribution we present new major and trace element data from the Kærven Syenite Complex (KSC) in East Greenland that provide geochemical evidence for the formation of cumulate rocks that are complementary to rhyolitic residual melts.

The development of the rifted continental margin and voluminous flood basalt volcanism in Palaeogene East Greenland included a multitude of intrusions of highly evolved magmas (e.g. Nielsen 1987; Riishuus *et al.* 2008; Brooks 2011). In the Kangerlussuaq area the world's largest syenite intrusion (the Kangerlussuaq Alkaline Intrusion – KAI) is accompanied by numerous smaller plutons (e.g. Riishuus *et al.* 2008), of which the Kærven Syenite Complex is one. Recent U-Pb zircon analyses (Thórarinsson *et al.* 2016) established the age of the entire complex, constrained the activity period, and enabled Kærven's geology to be regionally framed. The KSC is of Eocene age (see below) and illustrates processes during the early part of this period at a stage when basaltic activity in the Kangerlussuaq area was largely finished, and it displays the widest variation of rock types among the intrusive complexes of the province. The KSC is part of the development of magmatism in the Kangerlussuaq area at the time of waning influence from the passing Icelandic mantle plume with the establishment of the continent–ocean boundary and the formation of new ocean floor.

Holm & Prægel (1988a) presented the first more detailed geological, petrographical and geochemical data on the KSC. This minor but complicated intrusion had previously only received passing mention in the literature. Subsequent field work at Kærven (Holm *et al.* 1990) enabled us to map the area in some detail and to extend the sample database with additional geochemical information from locations not previously visited. A more comprehensive and updated treatment of the geological relations at Kærven is therefore appropriate. Furthermore, new comparisons can be made to the neighbouring KAI from which substantial amounts of data have been published since 1988 (e.g. Riishuus *et al.* 2008).

Based on field work conducted subsequent to our earlier accounts (Holm & Prægel 1988a, b; Holm 1990; Holm *et al.* 1991) we here record a sequence of eleven intrusive events in the formation of the KSC. We relate the geochemistry of the felsic rocks to the development and dynamics of the magmas and present a comprehensive account of the intrusive history and the magma chamber processes responsible for the lithological range in the KSC.

We present a model in which the main processes are differentiation by crystal accumulation during *in situ* crystallisation, followed by partial loss of interstitial liquid, and, in some units, accompanied by crustal contamination.

Geological setting

The extensive Palaeogene magmatic activity on the East Greenland continental margin encompasses a wide variety of extrusive and intrusive rock types, compositions and styles (Nielsen 1987). A significant number of the Tertiary complexes intruding the Archaean basement are exposed along the fjord Kangerlussuaq and further inland (e.g. Brooks 2011) and range from purely ultramafic (e.g. Kælvegletscher) over gabbroic (e.g. Skærgaard, Kap Edvard Holm) to entirely felsic bodies (e.g. Bagnæsset, Kræmer Ø, KAI). Ultramafic and felsic facies are developed in several gabbroic intrusions. Although several syenite intrusives in the Kangerlussuaq area are described from Kap Edvard Holm, Kap Deichmann, Kap Boswell and Barberkniven (Deer 1976; Deer *et al.* 1984), the Kærven Complex appears to be the only example displaying a coherent rock suite from monzonite to granite in addition to a gabbro unit.

The KSC is located approximately halfway up the south-western side of Kangerlussuaq fjord (Figs. 1, 2). Along its eastern and part of its northern margin, the KSC is bounded by the earlier, narrow Kærven Gabbro, which in turn is emplaced into Archaean basement gneisses (Holm *et al.* 2006). To the south the exposures of the KSC are bounded by the Nordre Syenitgletscher, and the western part of the complex is truncated by the KAI, which has removed parts of the complex. The KSC is exposed for 10 km along the perimeter of the KAI.

Rock types and field relations

The Kærven Syenite Complex (Fig. 1) is exposed on two relatively high-lying and steep-sided peaked plateaus of the Kærven mountain (English: Notch Mountain) (Fig. 2), here termed East Kærven (EK) and West Kærven (WK), in the interjacent partly snow-covered valley referred to as 'Vindhulsdalen' (informal name) and on the northern part of 'Eftermiddagstoppen' (informal name). The orientations of contacts between the units of the KSC indicate that quartz syenitic, syenitic and granitic magmas were emplaced as ring dykes in an assumed cauldron. Sills occur locally on West Kærven which further add to the impression that the KSC units were intruded in

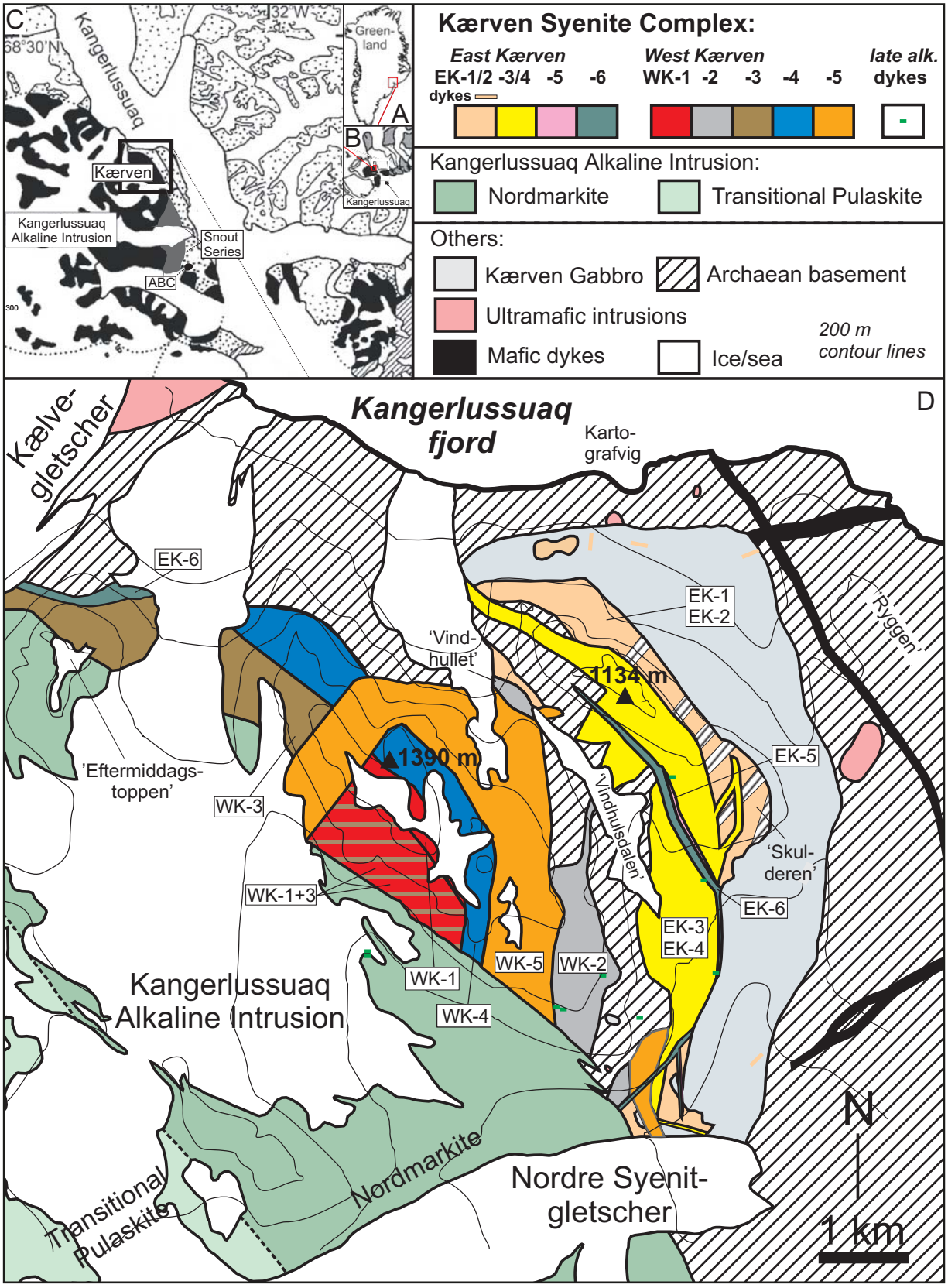

Fig. 1. Location map and geology of the Eocene Kærven Syenite Complex, Kangerlussuaq, East Greenland. Other Palaeogene intrusions of the Kærven area are also shown. **A**: Greenland. **B**: the triple junction of Kangerlussuaq and the 120° bend of the East Greenland coastline; Palaeogene flood basalts in grey and intrusions in black. **C**: Kærven situated at the edge of the Kangerlussuaq Alkaline Intrusion; ABC is Astrophyllite Bay Complex; Archaean basement is dotted. **D**: Geology of the Kærven Syenite Complex and immediate surroundings. Informal names of localities mentioned in the text are in inverted commas. Contour interval 200 m.

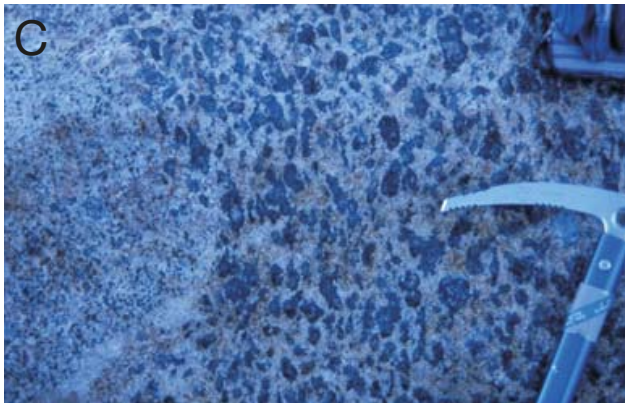

Fig. 2. A: Photo looking north from Kangerlussuaq fjord. In the background mount Kærven with the characteristic notch between East Kærven (right, 1134 m a.s.l.) and West Kærven (left, 1390 m a.s.l.) giving rise to its name, Notch mountain; **B**: Photo of the Kærven Syenite Complex from just north of Kælvegletscher looking south, showing from the left East Kærven and West Kærven (with sunny tops) and the north-western peak 'Eftermiddagstoppen', which displays the contact between the dark Kærven rocks and the light-coloured rocks of the Kangerlussuaq Alkaline Intrusion. See also map on Fig. 1D. **C**: Lobate contact between subunits of WK-4 alkali feldspar granite. Mafic inclusion-bearing, medium-grained hybrid granite (right) and medium-grained granite (left). See text for details.

response to cauldron sagging. Assuming an original circular form of the KSC, a minimum diameter of 10 km is indicated. The missing western part of such a ring complex was removed during emplacement of the magmas of the KAI. Eleven distinct intrusive units are recognised in the KSC (Fig. 1), ranging from quartz syenite (two closely related units EK-1 and EK-2) over syenite (WK-2) and quartz alkali feldspar syenites (EK-3 and EK-4, appearing as one in the field) to alkali feldspar granites (EK-5, EK-6, WK-1, WK-3, WK-4 and WK-5). Table 1 lists these units, their average mineral modes and IUGS rock classification (Le Maitre 1989). A suite of late alkaline dykes postdates the syenitic and granitic units. The following relative age relations were established during field work:

At East Kærven: Basement gneisses > Kærven gabbro > EK-1 > EK-2 > EK-3 ≥ EK -4 > EK-5 > EK-6 > late dykes (of green and grey varieties).

At West Kærven: WK-1 > WK-2 > WK-3 > WK-4 ≥ WK-5 > nordmarkite of the KAI > late dykes (green variety) > transitional pulaskite of the KAI.

Cross-cutting relationships in the area north of Nordre Syenitgletscher establish EK-3 and EK-4 syenites as contemporaneous with WK-2 syenites. The late green dykes were mapped in the nordmarkite but not in the transitional pulaskite of the KAI intrusion. The relative timing of this dyke event is therefore tentatively placed as shown.

Two representative rock photomicrographs are presented in Fig. 3. Petrographic details of Kærven rocks are given in Holm & Prægel (1988a). Sample localities are indicated on the map in Supplementary data file 2.

Basement and gabbro

Basement

Two Archaean (Bridgwater *et al.* 1978) basement outcrops in contact with the felsic Kærven rocks were investigated. One is located on the east side of the East Kærven peak and sits in the contact zone between the Kærven Gabbro and the EK-1 quartz syenite in which basement xenoliths are locally a volumetrically important part (see below). At 'Skulderen' the septum of basement between gabbro and EK-1 widens, but it is otherwise only a few metres wide and to the south of 'Skulderen' it is in contact with other units of KSC (Fig. 1). The second visited outcrop area of basement is exposed from north of Nordre Syenitgletscher to the saddle point at 'Vindhullet' at 750 m a.s.l.. The basement is predominantly composed of heterogeneous grey gneisses with granodioritic or tonalitic to granitic compositions with common streaks of amphibolite. Locally, the gneisses have experienced mobilisation and have a granitic texture. The basement gneisses in contact with KSC along its northern limits were

Table 1. Mineralogical compositions and types of rock units in the Kærven Syenite Complex and average basement gneiss in the Kærven area

	modal concentrations (vol. %)											QAPF classification			IUGS name
	alk f	plg	qz	ol	cpx	amph	bio	opq	apa	zir	tit	A	P	Q	
Average rock of unit												alk f	plg	qz	
Kærven															
EK-1	59	15	17	-	2	5	1	1	+	+	+	64.3	16.8	18.9	quartz syenite
EK-2	60	15	18	-	1	5	+	1	+	+	-	64.4	16.4	19.2	quartz syenite
EK-3	84	-	7	3	4	3	+	+	-	+	+	91.8	0.0	8.2	quartz alkali feldspar syenite
EK-4	72	1	14	2	4	6	+	+	-	-	-	82.4	1.7	15.9	quartz alkali feldspar syenite
EK-5	68	1	26	+	3	3	+	+	-	+	-	71.4	1.0	27.6	alkali feldspar granite
EK-6	70	+	23	+	2	5	+	+	-	-	+	75.6	0.0	24.4	alkali feldspar granite
WK-1	69	-	23	1	3	5	-	-	+	+	-	75.4	0.0	24.6	alkali feldspar granite
WK-2	71	3	13	+	5	6	2	+	+	+	-	81.2	3.7	15.1	quartz alkali feldspar syenite
WK-3	69	3	23	1	2	4	-	+	-	-	-	73.0	2.7	24.3	alkali feldspar granite
WK-4	57	-	40	-	-	3	+	-	-	-	-	58.8	0.0	41.2	alkali feldspar granite
WK-5	71	+	20	+	3	6	+	+	-	-	-	78.0	0.0	22.0	alkali feldspar granite
Basement gneiss	28	25	43	-	+	2	2	+	-	+	-	29.4	26.2	44.4	(monzo) granite

+ present, - not present, alk f - alkali feldspar, plg - plagioclase, qz - quartz, ol - olivine, cpx - clinopyroxene, amph - amphibole, bio - biotite, opq - opaque, apa- apatite, zir - zircon, tit - titanite

not reached except for on the north facing slope of 'Eftermiddagstoppen' where the basement contact at 450 m a.s.l. is vertical and oriented E–W.

Gabbro

The Kærven Gabbro floors the N–S trending valley between the basement complex at 'Ryggen' and the steep eastern cliffs of East Kærven (Fig. 1). To the north, the Kærven Gabbro exposure turns westward and disappears below the snow field north of 'Vindhullet' and west of the syenite outcrops, whereas the southern termination is obscured by the glacial moraines of Nordre Syenitgletscher. The Kærven Gabbro was described by Ojha (1966) and will not be treated further in the present work.

East Kærven

EK-1 and EK-2: Quartz monzodiorites to granites

These units were emplaced subsequent to the Kærven Gabbro and are the oldest members of the KSC. They were initially mapped as one, but geochemical data (see below) has prompted the division into two subunits.

EK-1 and EK-2 are heterogenous units with an overall average modal composition corresponding to quartz syenite; however, the units display significant internal lithological variations and include quartz monzodiorites, quartz monzonites, granodiorites, syenites and granites. Nevertheless, for simplicity we will refer collectively to the rocks from EK-1 and EK-2 as quartz syenites.

The subdivision of this unit is linked to macroscopic and/or geochemical evidence for contamination of the quartz syenites by basement and gabbro lithologies. These characteristics are observed in EK-1 rocks whereas EK-2 quartz syenites appear to have escaped major influence from the host rocks.

The dominant part of the EK-1/EK-2 unit is emplaced as a coherent body west of the Kærven Gabbro (Fig. 1) and intrudes the gabbro just north of Nordre Syenitgletscher. Minor EK-1/EK-2 occurrences appear as up to 7 m wide and variably inclined dykes in the gabbro. An isolated body of the quartz syenite unit, measuring approximately 100 × 300 m^2, is emplaced into the gabbro close to Kartografvig.

While internal contacts between EK-1 and EK-2 have not been observed, relatively large areas of the coherent quartz syenite body appear to consist of EK-1. Close to the eastern contact, the EK-1 brecciates the brittle basement above and west of the Kærven Gabbro, indicating that the basement gneiss roof of the gabbro intrusion was cold at the time of the EK-1 intrusion. Similarly, remobilised basement back-veins the gabbro but not the EK-1. In the 'Skulderen' area, the quartz syenite/gabbro contact is wavy, runs N–S and tends to be inclined slightly to the west. Quartz syenite dykes and sheets intrude the gabbro, e.g. at 'Skulderen', and close to the main contact the quartz syenite hosts gabbro inclusions. Detailed investigations at 'Skulderen' indicate that the quartz syenite intrusion here is composed of a number of relatively narrow, dyke-like, light coloured and heterogeneous bodies of variable width (1 m and less). They intrude basement gneiss and locally account for up to approximately 50% of the outcrops.

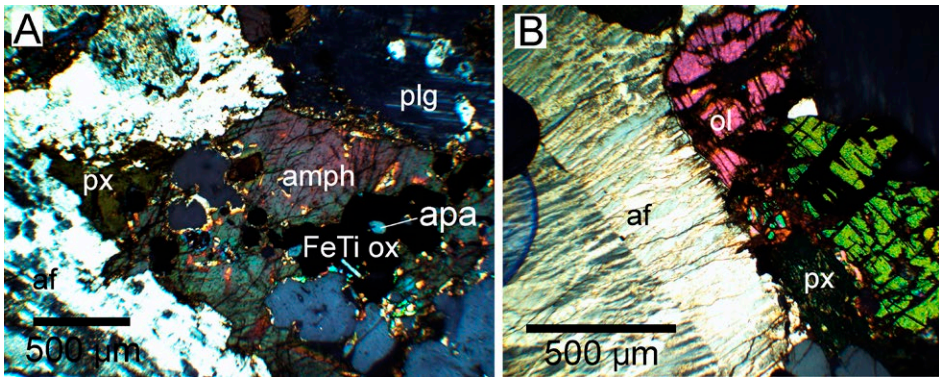

Fig. 3. Photomicrographs of selected Kærven quartz alkali feldspar syenites (cross polarised light). **A**: sample 66525 (WK-2); **B**: sample 66492 (EK-3). Alkali feldspar typically has mineral inclusions with interstitial clusters of mafic phases. af = alkali feldpar; plg = plagioclase; px = clinopyroxene; amph = amphibole; FeTi ox = typically ilmenite; apa = apatite; ol = olivine (for petrographic details see Holm & Prægel 1988a).

In the north-facing slopes of Kærven west of Kartografvig, the quartz syenite/gabbro contact is slightly undulating with a wavelength of a few metres and with a steep inward dip. The contact is buried beneath the snowfield north of 'Vindhullet'. In the exposures north of Kærven, the EK-1/EK-2 quartz syenites generally have a high proportion of basement xenoliths, some of which underwent near to total melting to yield a biotite granite at some time prior to their inclusion in their present host rocks.

Along the eastern contact to EK-3 syenites, a 50 m wide zone of quartz syenite is very rich in basement xenolith blocks. The basement seems to have been partially molten and contains porphyroblasts of feldspar and many rafts of amphibolite up to several metres long.

EK-3 and EK-4. Quartz alkali feldspar syenites

EK-3 is a conspicuous, reddish (often dark red) weathering medium-grained rock, which is prominent in the high-lying plateau south of the 1134 m eastern Kærven peak and extends south along the contact to the Kærven Gabbro and north along the EK-2 intrusion (Fig. 1). To the north-east, EK-3 forms a major part of the steep cliffs of the 1134 m peak, including the pinnacle-like erosional remnants high in the north-east facing rock slope (Fig. 2A). Owing to the steep relief, we did not conduct field work above app. 800 m a.s.l. in this area. Although field work did not prompt subdivision of this intrusive unit, geochemical data define a subtype, EK-4.

EK-5. Alkali feldspar granite

This is a small intrusion of fine-grained, whitish alkali feldspar granite which cuts EK-3 and is itself intruded by the EK-6 granite, which at places veins EK-5. The original size and form of this unit is unknown as only a wedge of few metres width of EK-5 is preserved after the emplacement of EK-6. EK-5 occasionally holds centimetre-sized rounded inclusions (enclaves) of fine-grained, more mafic syenite. EK-5 granites (along with WK-4 granites, see below) are the most evolved of the KSC rocks, composed of quartz and alkali feldspar and almost devoid of mafic phases (Table 1).

EK-6. Alkali feldspar granite

The EK-6 unit is a white to yellowish, up to 20–30 m wide ring-dyke-like body of medium-grained, feldspar-phyric alkali feldspar granite extending in an irregular way southwards from the northern end of 'Vindhulsdalen' where it cuts the basement. EK-6 magma was chilled against EK-3 syenites and EK-3 inclusions are occasionally found in EK-6. Likewise, the EK-6 magma was chilled against EK-5. EK-6 also shares a contact with the basement just south-east of Kælvegletscher at 'Eftermiddagstoppen', where it is presumed to be a dyke.

West Kærven

The West Kærven area constitutes the high ground around the western 1390 m peak of Kærven (Fig. 1). This western part of the KSC comprises many intrusive phases which are difficult to map as they occur as irregular bodies or as a multitude of sheets and dykes, though the southern part consists of more regular intrusive bodies. The exposed area west and south of the 1390 m peak appears to constitute the stoped roof zone of a syenitic magma chamber.

WK-1, WK-3 and WK-4. Alkali feldspar granites

The coarse-grained, reddish-weathering alkali feldspar granite WK-1 is the oldest intrusive unit at West Kærven. It is exposed in an area south and west of the 1390 m peak. To the south, this unit is intruded by the alkali feldspar granite WK-3 in the form of up to 20 m thick and brownish-weathering sills. Eastwards, WK-1 is cut by the alkali feldspar granite WK-4 (see below), in which it is found as xenoliths. At the foot of the southwestern face of the West Kærven massif, WK-1 is observed close to the contact with KAI.

WK-3 is a massive unit exposed north-west of the 1390 m peak. It is considered to represent the westernmost part of the KSC, as it probably also constitutes

most of the 'Eftermiddagstoppen' peak and terminates below the Kælvegletscher further to the west.

The West Kærven peak (1390 m) and the surrounding area consists predominantly of the complex WK-4 unit that includes at least three subunits with variable intrusive styles and petrographic appearances. The dominant subunit is a fine-grained, feldspar-phyric granite. The two additional subunits occur in the area south-east of the 1390 m peak and consist of a medium to coarse-grained granite and a medium-grained granite with centimetre-sized rounded mafic inclusions constituting up to 50% of the rock (Fig. 2C). The inclusion-bearing granite always occurs centrally and the medium-grained granite along the margins of the WK-4 unit. The rounded shapes of both the contact between the two medium-grained subunits and of the mafic inclusions clearly indicate mingling of magmas. The fine-grained porphyritic granite seems to be the earliest subunit in WK-4, whereas the two other subunits are broadly contemporaneous. A prominent occurrence of the porphyritic granite takes the form of a dyke that trends for 1 km and marks the eastern termination of WK-1 (Fig. 1). WK-3 and, more intensively, WK-1 are intruded by numerous WK-4 sills and dykes up to 5 m in width.

WK-2. Syenite

The WK-2 syenite is exposed in the high-lying ground north of Nordre Syenitgletscher and west of the basement segment in 'Vindhulsdalen'. It has the shape of an approximately N–S trending, 600 m wide dyke-like body. The WK-2 unit extends along the west slopes of 'Vindhulsdalen' to the north where it thins and turns into a NW–SE orientation. It is very likely that it crops out in the inaccessible north-facing cliffs of West Kærven that face the Kangerlussuaq fjord. WK-5 cuts WK-2 north-east of the contact with KAI.

WK-5. Alkali feldspar granite

The youngest unit in the KSC ring complex is WK-5. This medium- to coarse-grained alkali feldspar granite forms a 600 m wide, N–S trending dyke that cuts through the WK-2 unit and farther north is in contact with the Precambrian basement. The WK-5 granite resembles the neighbouring nordmarkites of the KAI with its conspicuous euhedral phenocrysts of microperthite (up to 5 cm) and the occurrence of interstitial quartz. Its southern part is emplaced between the porphyritic alkali feldspar granite dyke WK-4 and the WK-2 syenite unit. Further north the course of the WK-5 dyke changes to a NW–SE direction and also cuts the WK-1 to the south-west, where it developed a chilled contact rock. This intrusion appears to be the remnant of a ring dyke. A second dyke of WK-5 cuts NNE–SSW along the original contact of WK-1 and WK-3. Both dykes may continue north below glaciers at the north face of Kærven. It is noteworthy that valleys tend to be developed in the WK-5 granites that are susceptible to glacial abrasion, probably because of their relatively coarse grain size.

Dykes in the Kærven area

The Archaean basement surrounding the KSC is intruded by numerous steeply dipping, dark-weathering dykes with widths from < 1 m to > 30 m. Whereas the majority of sampled dykes are mafic and include tholeiitic basalts and trachybasalts, a suite of dykes with trachytic to rhyolitic compositions has also been mapped. We have no age constraints on either group of dykes, which are obviously not related to the magmatism of KSC and will not be treated further here.

Post-KSC and post-KAI dykes

While no mafic dykes have been found within the KSC, we discern two suites of late felsic dykes postdating the KSC and KAI. One suite consists of narrow (few decimetres wide), east to north-east striking vertical dykes with conspicuous green-coloured weathering surfaces due to aegirine. These dykes, with phonolitic or trachytic compositions, are aphyric and found occasionally throughout the KSC and in the adjoining basement. The green dykes are also present in the KAI nordmarkites but have not been observed in the transitional pulaskites. These dykes are considered unrelated to the magmatism of KSC but have clear geochemical bearings on the subsequent magmatic evolution of the KAI, and will be divided into groups 1 and 2. Green phonolitic dykes are common throughout the Kangerlussuaq region (Brooks 2011) and their possible relationship with those of the KSC is discussed below.

The second suite is of late, grey felsic dykes with trachytic to rhyolitic compositions which occur sporadically in the KSC. These dykes are compositionally similar to the felsic dykes mapped in the surrounding basement but are compositionally unrelated to KSC and not treated further in this contribution.

Relations to the Kangerlussuaq Alkaline Intrusion

The KSC is cut to the west by the medium- to coarse-grained nordmarkite of the KAI along a 10 km long NW–SE trending arcuate contact which curves to a N–S direction to the south (Fig. 1). The KAI nordmarkite contact turns to a NNW–SSE direction between the KSC and the Kælvegletscher Ultramafic Complex (Holm *et al.* 1991) and further north it arcs westwards. The numerous units truncated by the KAI

are, in sequence northwards from south of Nordre Syenitgletscher: Basement gneisses, EK-1/EK-2, EK-6, WK-2, WK-5, WK-4, WK-1 and WK-3. In places near the contact, the nordmarkite is lithologically different from the main part of the KAI intrusion, as it carries numerous centimetre- to decimetre-sized, rounded to angular, mafic inclusions or enclaves. This occurs both at the contact to WK-1 and to the Kælvegletscher Ultramafic Complex (Holm *et al.* 1990, 1991) on the north side of Kælvegletscher outside the area shown in Fig. 1. The nordmarkite is much less resistant to erosion (glacial abrasion) than most Kærven rocks, and the south-western contacts of Kærven units are marked by steep cliffs, except for 'Eftermiddagstoppen'.

Analytical methods

We present new major element analyses for 80 KSC rocks and new trace element analyses for 88 rocks. Also presented are new major and trace element analyses for local basement gneisses. A total of 95 petrographically fresh samples of KSC rocks and basement gneisses considered to be relatively unaltered were jaw crushed and subsequently powdered in a tungsten carbide mill. In addition, we re-analysed powders of some samples for which analytical data was previously published.

Major elements were analysed at GEUS (Geological Survey of Denmark and Greenland) by X-ray Fluorescence (XRF) analysis on a Philips PW 1606 spectrometer following Kystol & Larsen (1999). The rock powder was heated to 1000°C to determine the volatile content, measured as loss on ignition and corrected for oxidation of Fe. Si, Mg, Ti, total Fe, Mn, Ca, K and P were analysed in glass discs of sodium tetraborate and rock powder in the ratio 7:1. Na was analysed by atomic absorption spectrometry (AAS). The analytical precision of the data is (1σ absolute wt%) SiO_2: 0.15, TiO_2: 0.015, Al_2O_3: 0.05, Fe_2O_3: 0.1, MnO: 0.003, MgO: 0.05, CaO: 0.03, Na_2O: 0.05, K_2O: 0.005, P_2O_5: 0.005, and volatiles: 0.1.

Trace elements were analysed by one of the following methods:

(a) Inductively coupled plasma mass spectroscopy (ICP-MS) analysis of 41 KSC and four basement samples was carried out on a PerkinElmer 6100 DRC Quadrupole at GEUS after borate melting and dissolution in HF. Reproducibility of BCR-2 and BHVO-2 at 1σ level was better than 2 rel.% for Ga, Rb, Sr, Y, Zr, Nb, Ba, La, Ce, Pr, Nd, Sm, Gd, Tb, Er, Dy, Ho, Yb, Lu, Ta, Th; and 2–3 rel.% for Mn, Tm and U, 3–5 % for Sc, Ti, V, Zn, Ni, Co, Ta. Determination of Cu seems less reliable by the borate melting method, and Cr reproduced with 15 rel.% (1σ) and Pb with 8 rel.%. Abundances of all elements discussed in this paper deviate less from the GeoReM preferred Values (Jochum and Nehring 2006) than the 2σ reproducibility. Documentation for the analytical quality is presented in Supplementary data file 1.

(b) Trace element analysis by XRF of 39 KSC and 10 basement samples was carried out on pressed powder pellets using a Philips PW 1400 instrument at the Department of Geosciences and Natural Resource Management, University of Copenhagen. The international standards G-2, GSP-1, AGV-1, W-1, BCR-1, PCC-1 and DTS-1 were used for calibration and AGV-1 as monitor. Reproducibility of AGV-1 was as follows: For Nb, Zr, Rb, Sr, Ce, La and Ba: *c.* 2 rel.%; Nd, Y, Zn, Cu, Ga, V, Cr, Sc: ≈5 rel.%; Th and Pb: 20 rel.% (1σ).

(c) Instrumental neutron activation analysis (INAA) was carried out on a subset of 8 KSC and 2 basement samples, using a Ge detector on a multichannel analyser at the Geological Institute (Gwozdz *et al.* 1993) on 100 mg powder irradiated at the Danish Nuclear Research Reactor at Risø. Iron was used for calibration and the analytical quality monitored by BHVO-1 with a reproducibility for Sc, Zn, La, Ce, Eu, Hf, Ta and Th below 1 rel.% (1σ), for Rb, Ba, Nd, Sm, Tb, Yb, Lu at 2–5 rel.% and for Cs at 7 rel.%.

Geochemical results

The nine intrusive units of the KSC identified in the field, plus the subsequent subdivisions of quartz syenites (EK-1/EK-2) and syenites (EK-3/EK-4) at East Kærven based on geochemistry (11 units in all), can be discerned by their major and trace element compositions. Table 2 lists major and trace element analyses of selected rocks from each unit (complete listing in Supplementary data file 1). Selected Harker diagrams for the Kærven rocks are presented in Fig. 4 where compositional fields are shown for the neighbouring KAI as defined by the analyses of Riishuus *et al.* (2008) and for local basement gneisses (analyses are listed in Supplementary data file 1).

With the exception of late dykes, all units of the KSC are quartz-bearing. The KSC rocks are typically alkaline (in terms of the modified alkali-lime index $Na_2O + K_2O - CaO$) and metaluminous (Fig. 4P), following the granite classification scheme of Frost *et al.* (2001). A few intermediate EK-3 rocks and a number of more silicic EK-6, WK-3, and WK-4 samples are peralkaline, whereas quartz syenites are generally metaluminous and alkali-calcic. The most Si-rich of the KSC units (EK-5, EK-6, and WK-4) trend from alkaline to alkali-calcic.

The late dykes in KSC have 6–10 % CIPW-normative *ne*. These dykes are peralkaline and classify as phonolites and trachytes on a TAS diagram (Fig. 4O).

The geochemical signature of the local Archaean basement in the Kærven area is clearly different from the intrusives in being peraluminous, magnesian and showing a range of calcic to alkali-calcic compositions with relatively low K_2O, FeO^{total} and MnO.

The total alkali vs. silica diagram (Fig. 4O) illustrates the geochemical variation and identifies the mapped units of the Kærven complex. With increasing SiO_2 these units are: WK-2 + EK-2, EK-1, EK-3 + EK-4, WK-1, WK-5, WK-3, EK-6, WK-4, and EK-5. Total alkalis build up irregularly in WK-2, EK-2, WK-1, WK-3, and WK-5, reach a maximum of *c*. 11 wt% $Na_2O + K_2O$ in the EK-6 granites at 68 wt% SiO_2 and taper off to 9.5 wt% alkalis at 74 wt% SiO_2 in the remaining rocks from this unit and in granites from units WK-4 and EK-5.

The compositional variation of the Kærven complex is compared to that of the KAI (Riishuus *et al*. 2008) in Fig. 4. Rocks with > 71 % SiO_2 are restricted to the KSC, whereas rocks with < 58 % SiO_2 characterise the KAI foyaites. In addition, the foyaites and the late green dykes have higher Na_2O for their SiO_2 than the KSC rocks. Contrary to the Kærven case, the bulk of the rock volume in the KAI is peralkaline (Fig. 4P) and tends to be more alkali-rich and iron-poor than the KSC rocks with corresponding SiO_2. We note some compositional overlaps between KSC and KAI, e.g. FeO^{total} and Al_2O_3 at intermediate SiO_2 levels. However, high Na_2O and low CaO distinguish the KAI from the KSC, and total alkalis in the KAI diverge significantly from the KSC (Fig. 4O), as, at similar SiO_2 below 65 %, KAI units (i.e. the transitional pulaskites and main pulaskites of the central parts of KAI) have distinctly higher total alkalis than any Kærven unit. Moreover, the transitional pulaskites, main pulaskites and foyaites of KAI have at least 2 wt% less FeO^{total} than Kærven rocks at any silica content, while displaying significantly higher Al_2O_3 than KSC rocks with similar SiO_2. The late dykes mainly plot between the main pulaskite unit and the central unit of foyaite from the KAI (see e.g. Riishuus *et al*. 2008).

A comparison with other intrusions along Kangerlussuaq fjord nearer to the ocean shows that the least evolved samples from the heterogeneous Kræmer Ø syenite (Brooks 1991) plot with the Kærven units EK-3/EK-4 and the most felsic with EK-6. Syenites from the Astrophyllite Bay Complex (ABC, Fig. 1C) (Riishuus *et al*. 2005) tend to have similar to slightly higher alkalis than comparable KSC rocks, and specifically the high Na_2O in ABC suggests a relationship with the KAI. Similar high contents of alkalis are seen in Snout Series syenites from the Astrophyllite Bay area (Riishuus *et al*. 2006), while Snout series syenites from the area north of Søndre Syenitgletscher analysed by Deer & Kempe (1976) have quite divergent compositions, plotting either with Kærven EK-1/EK-2 quartz syenites or trending towards more mafic compositions. Syenite bodies are found near the mouth of Kangerlussuaq fjord (Fig. 1B) at Kap Deichmann, Barberkniven and Kap Boswell (Deer *et al*. 1984). None of these intrusions display a complete differentiated sequence from syenite to granite as seen at Kærven. Primitive Kap Deichmann syenites have low TiO_2, high Al_2O_3 and higher total alkalis than their Kærven counterparts and trend towards the high total alkalis fields of Kap Boswell and ABC syenites.

For reference we show the data fields of tholeiitic Icelandic volcanic rocks as extracted from the GEOROC (2018) database in variation diagrams in Figs. 4F, H and O. We compare with Icelandic compositions because the Icelandic mantle plume has been argued to be responsible for early Tertiary magmatism at the East Greenland margin, e.g. Brooks (1973) and White & McKenzie (1989). The impediment of such a comparison due to crystal accumulation at KSC is discussed below. In the TAS diagram (Fig. 4O), KSC rocks with up to 70 wt% SiO_2 have far higher total alkalis than Icelandic volcanic rocks including Thingmuli as defined by Carmichael (1964) and Charreteur *et al*. (2013).

The Harker diagrams in Fig. 4 effectively illustrate the chemical variation of the KSC, the geochemical characteristics of the individual intrusive units, as well as the overall distinction of the KSC from the KAI and Icelandic rocks. With SiO_2 increasing from 60 to 74 wt%, the overall geochemical variation of KSC

▶ **Fig. 4** *(two pages).* Major element variation of the Kærven Syenite Complex (Table 2 and Supplementary data file 1). Mg# = atomic 100Mg/(Mg + Fe^{2+}). ASI: Aluminium Saturation Index (molar values, Zen 1986). PI: Peralkalinity Index, molar values. Fields for the Kangerlussuaq Alkaline Intrusion are shown in selected diagrams: F: foyaites, MP: main pulaskites, TP: transitional pulaskites, N: nordmarkites, and QN: quartz nordmarkites (Riishuus *et al.* 2008). Fields for local basement gneisses of this study (Supplementary data file 1) are also shown. The trend of the Thingmuli volcanic rocks from Iceland (Carmichael 1964; Charreteur *et al*. 2013) is shown for reference in **C** as well as tholeiitic rocks of Iceland from the GEOROC (2018) database in **F**, **H**, and **O**. Proposed magmatic evolution trends for Icelandic magmas according to Charreteur *et al.* (2013) are shown in **J**. LLD is a calculated liquid line of descent for a tholeiitic basalt under reduced conditions using the MELTS software package (Ghiorso & Sack 1995). Numbers of two WK-2 samples discussed in the text are shown in some diagrams.

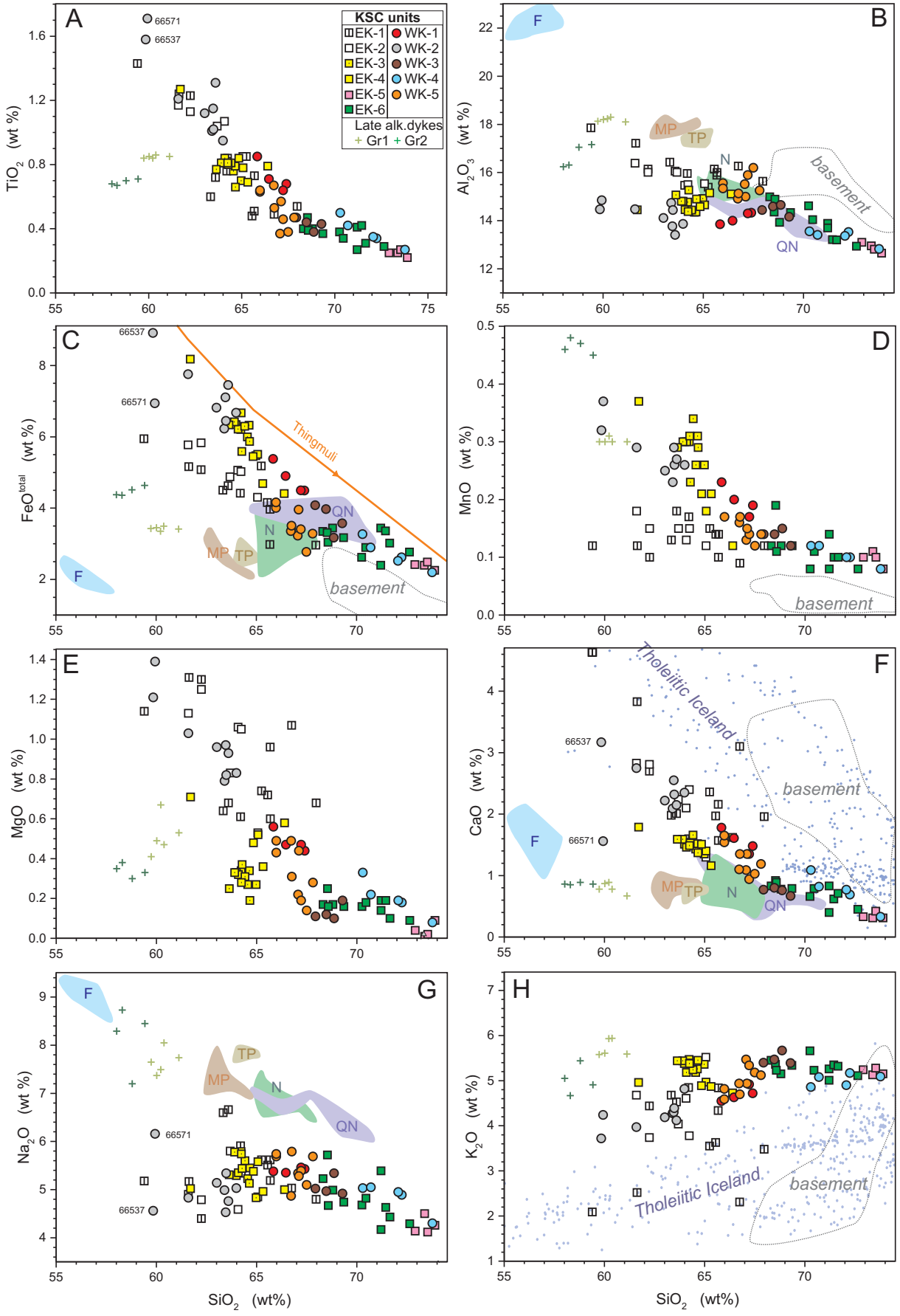
A
B
C
D
E
F
G
H
KSC units
EK-1
EK-2
EK-3
EK-4
EK-5
EK-6
WK-1
WK-2
WK-3
WK-4
WK-5
Late alk.dykes
Gr1
Gr2
66571
66537
F
MP
TP
N
QN
basement
Thingmuli
Tholeiitic Iceland
TiO2 (wt %)
Al2O3 (wt %)
FeOtotal (wt %)
MnO (wt %)
MgO (wt %)
CaO (wt %)
Na2O (wt %)
K2O (wt %)
SiO2 (wt%)

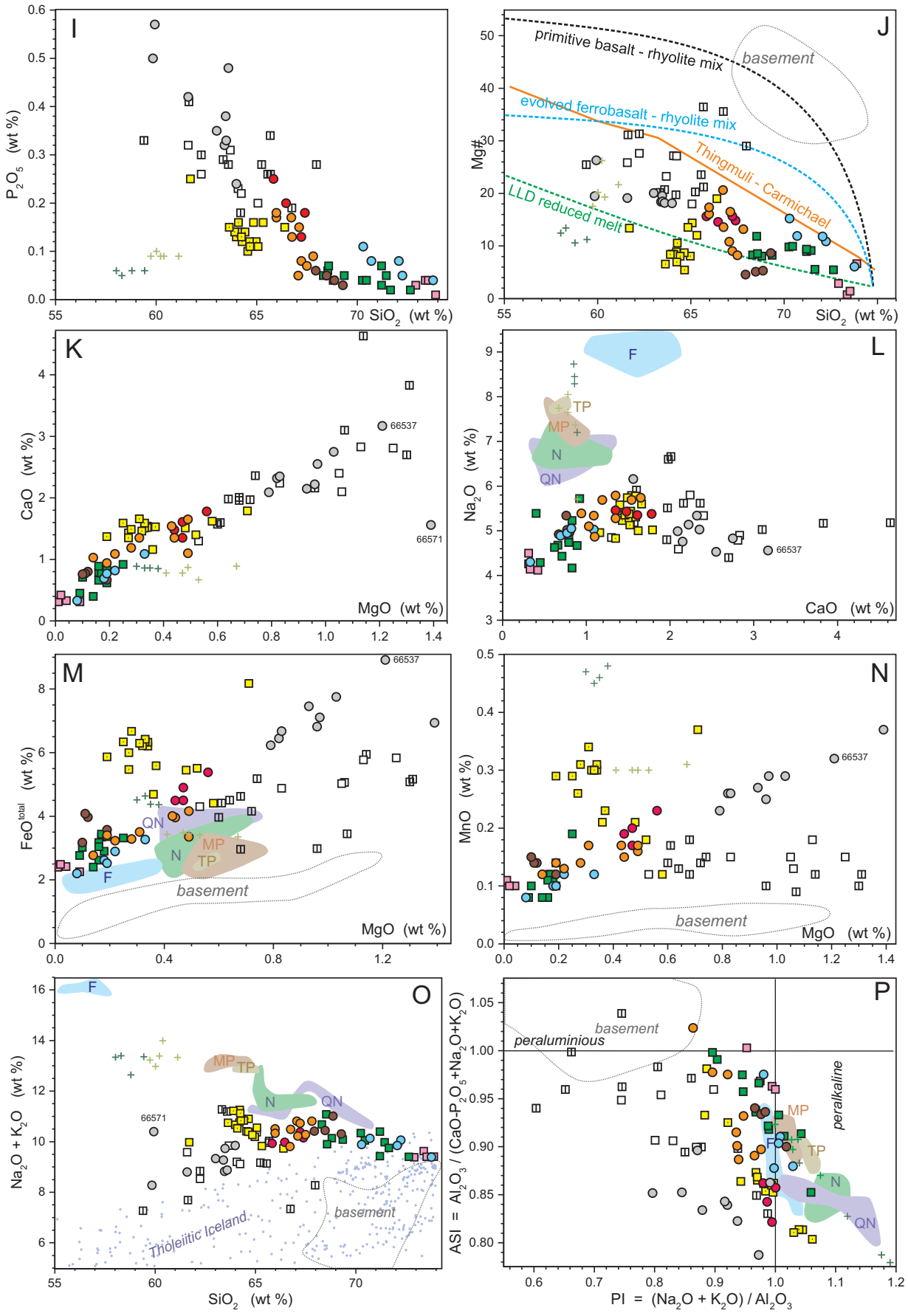
I
P2O5 (wt %)
SiO2 (wt %)
J
Mg#
primitive basalt - rhyolite mix
basement
evolved ferrobasalt - rhyolite mix
Thingmuli - Carmichael
LLD reduced melt
SiO2 (wt %)
K
CaO (wt %)
66537
66571
MgO (wt %)
L
Na2O (wt %)
F
TP
MP
N
QN
66537
CaO (wt %)
M
FeOtotal (wt %)
66537
QN
MP
N
TP
F
basement
MgO (wt %)
N
MnO (wt %)
66537
basement
MgO (wt %)
O
Na2O + K2O (wt %)
F
MP
TP
N
QN
66571
Tholeiitic Iceland
basement
SiO2 (wt %)
P
ASI = Al2O3 / (CaO-P2O5+Na2O+K2O)
basement
peraluminious
peralkaline
MP
TP
N
QN
PI = (Na2O + K2O) / Al2O3

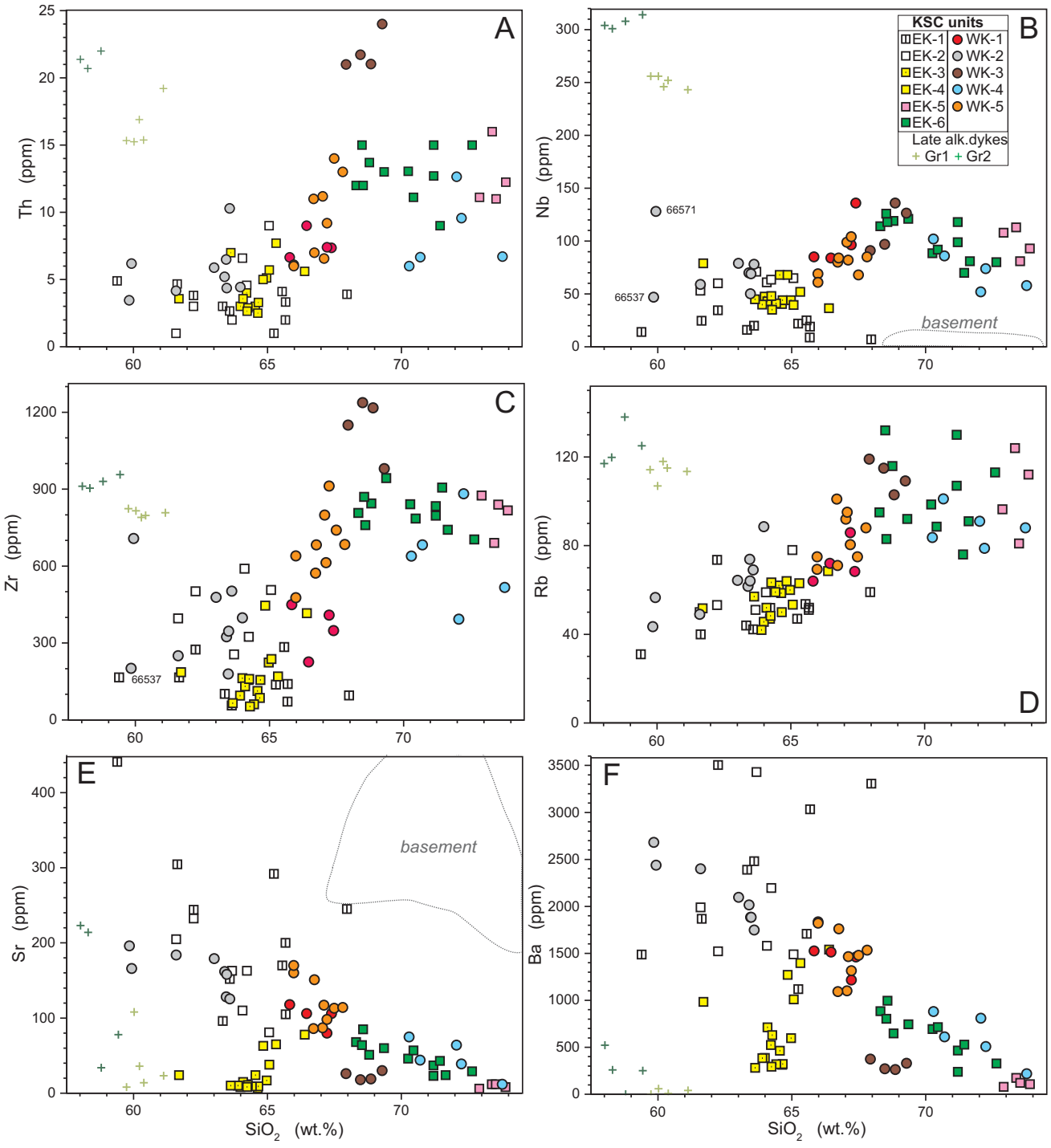

Fig. 5 *(two pages).* Trace element variation of KSC rocks. The field of local basement rocks is indicated in **B** and **E**, where the contrast to KSC is particularly distinct. Numbers of two WK-2 samples discussed in the text are shown in some diagrams.

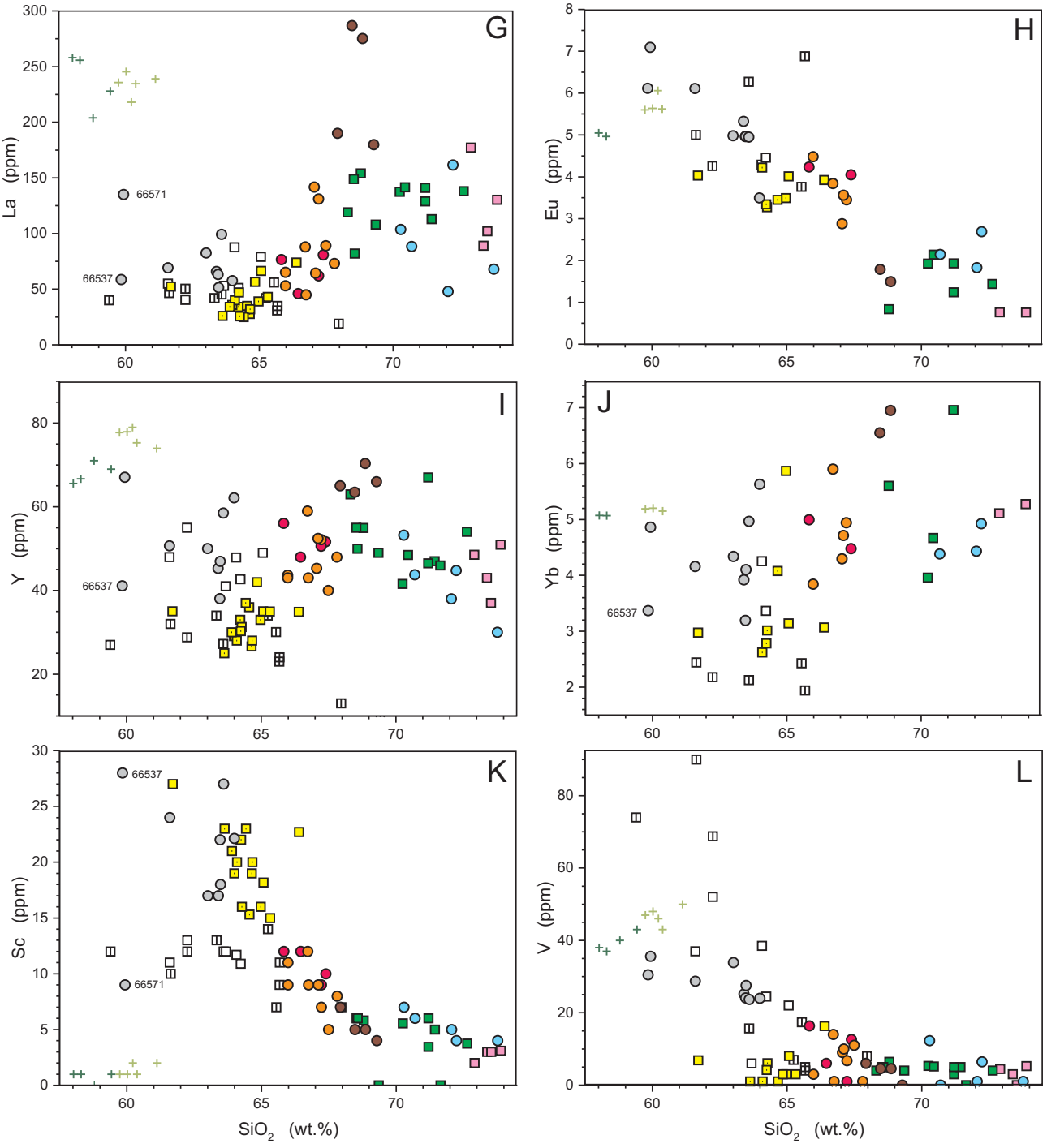
G
La (ppm)
66571
66537
H
Eu (ppm)
I
Y (ppm)
66537
J
Yb (ppm)
66537
K
Sc (ppm)
66537
66571
SiO2 (wt.%)
L
V (ppm)
SiO2 (wt.%)

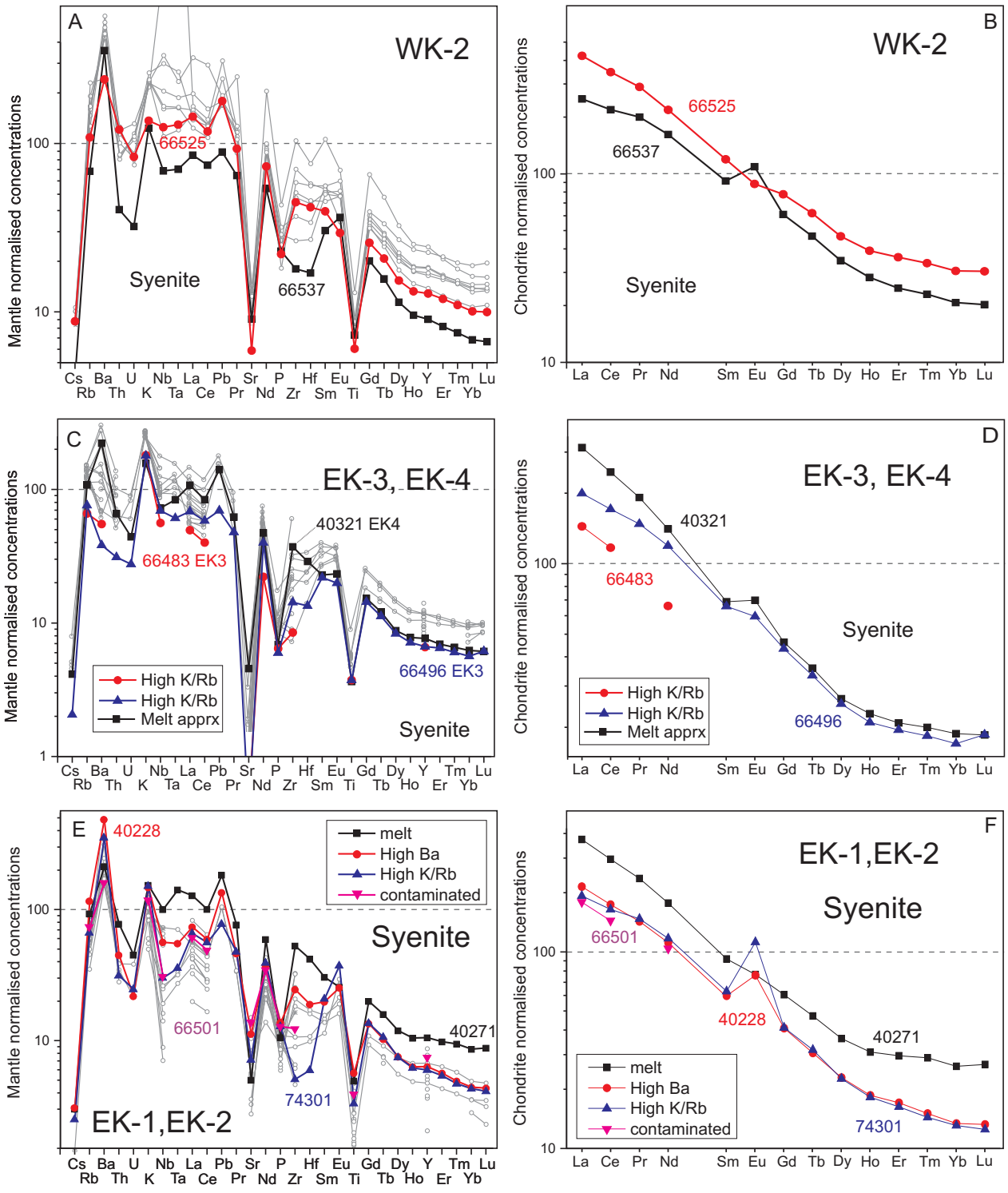

Fig. 6 *(two pages).* Mantle normalised multielement diagrams and chondrite normalised rare earth element diagrams for KSC rocks and local basement gneisses. Thick lines are for approximate melt compositions and for strongly accumulative rocks. Other individual rocks are with grey lines. Of the late dykes in panel K, Group 2 has relatively low K, HREEs, Y, and high Nb, Zr. See text for discussion. Normalising values from Sun & McDonough (1989).

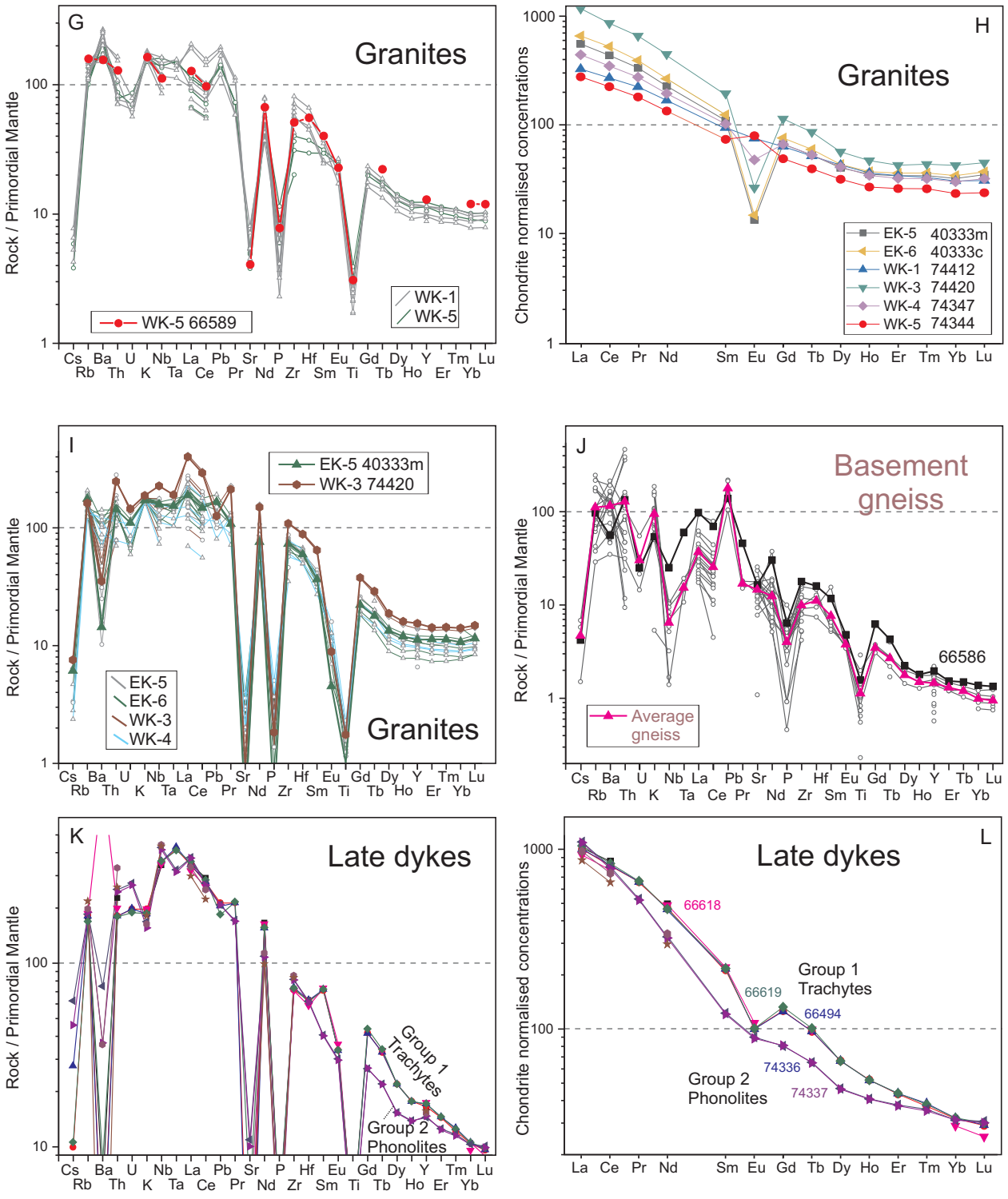
G
Granites
Rock / Primordial Mantle
WK-5 66589
WK-1
WK-5
H
Granites
Chondrite normalised concentrations
EK-5 40333m
EK-6 40333c
WK-1 74412
WK-3 74420
WK-4 74347
WK-5 74344
I
EK-5 40333m
WK-3 74420
EK-5
EK-6
WK-3
WK-4
Granites
J
Basement gneiss
66586
Average gneiss
K
Late dykes
Group 1 Trachytes
Group 2 Phonolites
L
Late dykes
66618
66619
66494
74336
74337
Group 1 Trachytes
Group 2 Phonolites

Table 2. Representative major and trace element rock analyses of the Kærven Syenite Complex

	East Kærven												
	EK-1	EK-1	EK-1	EK-2	EK-2	EK-3	EK-3	EK-4	EK-4	EK-5	EK-5	EK-6	EK-6
Sample no.	40228*	66550**	66580	40271*	40304	66467	66496	40321	40330**	40333m	66493	40333c	66495**
Rock type	Gra	Qz monz	Granod	Af gra	Qz af sy	Qz af sy	Qz af sy	Qz af sy	Qz af sy	Af gra	Af gra	Af gra	Af gra
SiO_2 wt. %	62.24	65.55	61.63	64.07	64.23	64.97	64.24	66.39	65.07	73.89	73.38	68.80	71.20
TiO_2	1.23	0.48	1.24	1.07	0.84	0.70	0.81	0.79	0.78	0.22	0.25	0.40	0.41
Al_2O_3	16.14	16.14	17.22	15.47	15.50	14.92	14.38	15.11	14.65	12.65	12.95	13.93	13.89
Fe_2O_3	2.30	1.92	2.56	1.77	1.52	1.60	3.48	2.01	1.92	1.15	0.93	1.19	1.58
FeO	3.01	2.43	2.86	3.47	3.66	4.03	3.54	2.60	3.78	1.22	1.56	2.37	2.02
FeO*	5.08	4.16	5.16	5.06	5.03	5.47	6.67	4.41	5.51	2.25	2.40	3.44	3.44
MnO	0.10	0.14	0.12	0.13	0.15	0.26	0.31	0.12	0.18	0.08	0.11	0.12	0.14
MgO	1.30	0.72	1.31	1.06	1.05	0.27	0.28	0.58	0.52	0.09	0.01	0.17	0.19
CaO	2.70	1.97	3.83	2.10	2.40	1.35	1.49	1.62	1.40	0.31	0.31	0.78	0.83
Na_2O	4.40	5.51	5.17	4.59	5.34	4.83	5.74	5.00	5.58	4.26	4.50	4.99	4.17
K_2O	4.44	3.63	2.52	4.61	3.78	5.36	5.38	4.73	4.97	5.15	5.13	5.15	5.26
P_2O_5	0.30	0.26	0.41	0.23	0.22	0.12	0.13	0.15	0.11	0.01	0.04	0.04	0.07
LOI	0.88	0.51	0.41	0.46	0.66	0.52	0.23	0.24	0.8	0.11	0.31	0.41	0.48
Total	98.81	99.07	99.02	98.85	99.20	98.77	99.66	99.14	99.57	99.02	99.39	98.23	100.08
Sc ppm	**12**	**7**	**10**	12	11	**16**	**7**	23	18	**3**	**3**	*6*	**6**
V	68.75	17.39	**90**	38.48	24.50	**3**	4.19	16.33	8.03	5.28	**3**	6.44	**3**
Cr	6.55	3.56	**6**	7.52	13.60	**0**	1.78	4.72	2.11	2.10	**0**	8.56	**2**
Co	38.82	39.48	**49**	17.59	43.21	**37**	30.59	40.16	32.84	72.14	**65**	77.93	**61**
Ni	10.77	4.45	**7**	9.61	11.89	**0**	3.56	5.53	3.43	3.34	**2**	6.14	**1**
Cu	56.66	42.09	**20**	53.71	55.49	**8**	42.07	37.89	64.21	30.64	**1**	30.53	**1**
Zn	76.42	103.13	**79**	112.84	102.81	**115**	111.99	97.83	125.01	86.42	**101**	90.84	**137**
Ga	24.40	27.46	**25**	28.66	27.73	**27**	29.69	26.81	28.59	29.74	**27**	29.35	**26**
Rb	73.55	53.65	**40**	58.96	51.90	**60**	48.30	68.53	53.39	112.00	**124**	115.91	**107**
Sr	237.49	165.89	**305**	105.66	160.17	**17**	7.64	96.07	45.70	8.55	**12**	12.85	**37**
Y	28.82	30.06	**32**	47.91	42.71	**33**	30.30	34.87	35.02	50.94	**43**	54.96	**67**
Zr	274.31	284.40	**166**	590.32	324.22	**224**	159.98	416.18	237.93	817.30	**690**	844.62	**834**
Nb	40.17	26.00	**25**	71.39	72.29	**44**	49.45	51.88	58.46	112.83	**113**	116.72	**118**
Cs	0.24	0.32		0.24	0.16		0.16	0.33	0.24	0.48		0.61	
Ba	3388	1662	**1868**	1484	2118	**596**	268	1552	977	100	**175**	111	**466**
La	50.45	56.02	*46.6*	87.56	51.09	**39**	47.02	73.91	66.36	130.30	**89**	154.03	**129**
Ce	104.98	108.91	*92.0*	178.37	108.01	**80**	103.60	149.19	138.21	262.81	**199**	316.69	**250**
Pr	12.74	12.97		21.06	13.12		13.22	17.15	17.28	29.80		34.92	
Nd	50.41	49.72	*53.3*	80.14	52.09	**50**	54.16	63.93	66.85	102.90	**73**	120.45	**110**
Sm	8.78	8.51	9.05	13.52	9.66	*10.1*	9.71	10.16	11.67	16.24		18.30	
Eu	4.26	3.76	*5.00*	4.29	4.46	*3.49*	3.34	3.93	4.01	0.76		0.84	*1.93*
Gd	8.04	7.71		11.91	9.00		8.55	9.11	10.03	13.18		14.97	
Tb	1.111	1.119	*1.14*	1.714	1.370	*1.35*	1.214	1.306	1.411	1.927		2.174	*2.59*
Dy	5.57	5.70		8.79	7.62		6.14	6.45	7.34	9.87		10.61	
Ho	1.037	1.110		1.719	1.532		1.173	1.277	1.352	1.966		2.082	
Er	2.72	2.87		4.71	4.23		3.11	3.33	3.53	5.44		5.75	
Tm	0.364	0.405		0.700	0.591		0.447	0.486	0.503	0.833		0.881	
Yb	2.18	2.43	*2.44*	4.26	3.37	*3.29*	2.78	3.07	3.14	5.28		5.60	*6.96*
Lu	0.322	0.360	*0.324*	0.650	0.490	*0.463*	0.454	0.453	0.476	0.853		0.906	*0.857*
Hf	5.84	6.89	*4.63*	12.95	7.36	*5.87*	4.16	8.92	6.84	18.39		18.67	*20.9*
Ta	2.260	1.808	*1.89*	5.788	4.028	*3.12*	2.500	3.435	3.137	6.291		5.990	*7.25*
Pb	9.55	10.20		12.99	10.36		4.93	10.00	8.37	11.77		13.66	
Th	3.82	4.10	*4.67*	6.59	4.56	*5.1*	2.64	5.60	5.71	12.23	**16**	13.70	**15**
U	0.458	0.629		0.944	1.117		0.578	0.927	1.242	2.316		2.480	

Number in bold: analysis by XRF, in italics: inaa, other: by icp-ms. Asterisk: major element data reported by Holm & Prægel (1988a).
Double asterisk: major element data reported by Holm et al. (1991).

Table 2. Continued

		West Kærven										Late dykes	
	EK-6	WK-1	WK-1	WK-2	WK-2	WK-3	WK-3	WK-4	WK-4	WK-5	WK-5	Trachytic	Phonolitic
Sample no.	40325	74412	74419	66525**	66537	66614	74420	74347	74414	66596	74344	66480	74337
Rock type	Af gra	Af gra	Af gra	Sy	Sy	Af gra	Af gra	Af gra	Af gra	Af gra	Af gra	Pho	Pho
SiO_2 wt. %	70.45	65.83	67.39	63.59	59.84	67.93	68.86	70.29	70.70	67.49	65.98	60.38	58.30
TiO_2	0.34	0.85	0.68	1.31	1.58	0.47	0.38	0.50	0.42	0.38	0.63	0.86	0.67
Al_2O_3	14.04	13.85	14.33	13.41	14.47	14.44	14.65	13.56	13.41	16.20	15.56	18.30	16.31
Fe_2O_3	0.62	1.37	1.03	3.13	3.53	1.76	1.07	0.79	0.73	1.17	1.13	0.05	0.79
FeO	2.34	4.15	3.57	4.64	5.74	2.50	2.21	2.56	2.24	1.72	2.99	3.83	3.97
FeO*	2.90	5.38	4.50	7.46	8.92	4.08	3.17	3.27	2.90	2.77	4.01	3.50	4.36
MnO	0.11	0.23	0.19	0.27	0.32	0.14	0.15	0.12	0.12	0.12	0.17	0.30	0.48
MgO	0.18	0.56	0.44	0.93	1.21	0.11	0.10	0.33	0.22	0.14	0.43	0.47	0.38
CaO	0.79	1.78	1.48	2.15	3.17	0.77	0.76	1.09	0.82	1.03	1.54	0.78	0.85
Na_2O	4.82	5.38	5.43	4.76	4.56	5.02	5.34	5.03	5.05	5.10	5.69	8.05	8.73
K_2O	5.23	4.55	4.72	4.12	3.72	5.40	5.67	4.86	5.08	5.18	4.82	5.94	4.67
P_2O_5	0.04	0.25	0.18	0.48	0.50	0.06	0.04	0.11	0.08	0.07	0.17	0.09	0.05
LOI	0.48	0.72	0.5	0.77	0.59	0.37	0.61	0.56	0.65	0.45	0.5		2.43
Total	99.38	99.38	99.84	99.25	98.88	98.79	99.73	99.72	99.45	98.93	99.50	99.05	97.63
Sc ppm	*6*	**12**	**10**	**27**	**28**	**7**	**5**	**7**	**6**	**5**	**9**	**1**	**1**
V	5.34	16.38	12.62	23.69	30.50	**6**	4.54	12.30	7.38	**11**	14.29	50.23	47.76
Cr	2.77	1.50	6.91	1.63	13.65	**8**	1.13	1.39	2.61	**0**	1.62	1.84	2.69
Co	66.47	21.73	28.49	29.57	28.84	**44**	27.70	22.17	41.47	**40**	29.19	20.09	22.84
Ni	4.38	4.33	3.96	3.97	10.38	**1**	2.67	3.77	3.92	**2**	3.31	3.48	2.87
Cu	41.35	56.40	51.49	61.64	71.13	**0**	38.82	50.13	57.15	**0**	50.22	44.10	50.04
Zn	80.50	126.63	112.39	151.85	152.92	**122**	103.81	98.08	81.37	**82**	98.92	164.16	119.57
Ga	30.62	29.44	28.92	29.06	26.67	**30**	33.54	29.97	30.92	**26**	29.86	37.04	38.67
Rb	98.58	64.00	68.34	69.04	43.45	**119**	102.94	83.69	101.11	**75**	69.27	115.04	119.76
Sr	52.44	115.36	103.35	124.51	191.35	**26**	19.66	75.55	42.64	**113**	162.83	14.80	211.38
Y	41.58	56.07	51.67	58.54	41.12	**65**	70.34	53.23	43.74	**40**	43.67	75.30	66.69
Zr	841.00	449.31	348.40	502.43	201.51	**1150**	1216.82	638.72	682.72	**740**	640.11	797.76	904.08
Nb	112.14	99.48	114.68	89.23	49.02	**91**	161.90	112.87	91.94	**68**	82.65	254.64	294.37
Cs	0.52	0.46	0.30	0.69	0.32		0.60	0.26	0.49		0.52	0.78	3.62
Ba	706	1499	1458	1682	2496	**374**	246	865	612	**1480**	1869	15	256
La	137.46	76.61	80.85	99.18	58.62	**190**	275.31	103.63	88.31	**89**	65.17	234.72	255.78
Ce	272.22	163.18	169.48	209.27	132.06	**361**	518.57	210.66	181.77	**182**	135.92	487.02	469.80
Pr	29.70	20.00	20.17	25.75	17.82		58.54	24.57	19.83		16.15	58.72	46.51
Nd	102.40	76.29	75.27	98.94	73.15	**146**	202.46	88.02	71.45	**78**	61.07	211.46	145.39
Sm	14.81	13.90	13.11	17.59	13.50		28.64	15.08	12.11		10.92	31.40	17.77
Eu	1.93	4.24	4.05	4.95	6.11		1.49	2.69	2.15		4.48	5.62	4.96
Gd	11.72	12.53	11.80	15.33	11.96		22.48	13.11	10.94		9.68	24.84	15.92
Tb	1.654	1.890	1.789	2.244	1.70		3.128	1.938	1.626		1.443	3.516	2.354
Dy	7.75	10.45	9.36	11.31	8.42		13.82	10.06	8.29		7.73	16.16	11.22
Ho	1.473	2.024	1.823	2.172	1.57		2.631	1.926	1.64		1.51	2.90	2.26
Er	4.08	5.46	4.88	5.73	3.93		6.84	5.17	4.43		4.16	6.91	5.93
Tm	0.613	0.802	0.711	0.814	0.56		1.062	0.781	0.659		0.631	0.899	0.849
Yb	3.96	5.00	4.48	4.97	3.37		6.95	4.92	4.38		3.84	5.15	5.07
Lu	0.623	0.752	0.655	0.739	0.49		1.097	0.784	0.688		0.582	0.707	0.730
Hf	18.50	11.48	9.16	12.95	5.26		27.33	15.87	15.43		13.82	19.37	18.84
Ta	6.622	6.248	5.980	5.317	2.89		7.815	6.034	4.928		4.614	17.122	12.835
Pb	12.25	9.76	10.09	12.68	6.32		8.92	8.04	9.58		8.48	15.12	14.73
Th	13.05	6.65	7.36	10.29	3.45	**21**	21.03	9.56	6.67	**14**	6.10	15.37	20.69
U	1.249	1.810	1.462	1.753	0.68		3.041	2.297	1.514		1.353	4.134	5.568

Abbreviated rock type names: Granod: Granodiorite, Sy: syenite, Gra: Granite, Qz af sy: Quartz alkali feldspar syenite, Tra: Trachyte, Qz monz:Quartz monzonite, Af gra: Alkali feldspar granite, Pho: Phonolite

displays trends of decreasing TiO_2, FeO^{total}, MnO, CaO, and P_2O_5. Individual Kærven intrusive units, however, follow separate trends which are not all subparallel. Moreover, the geochemical variations in the low-SiO_2 part (*c.* 60–66 % SiO_2) of the KSC, encompassing the EK-1, EK-2, WK-2, EK-3 and EK-4 units, show significantly divergent trends with respect to Al_2O_3, MgO, MnO, and K_2O.

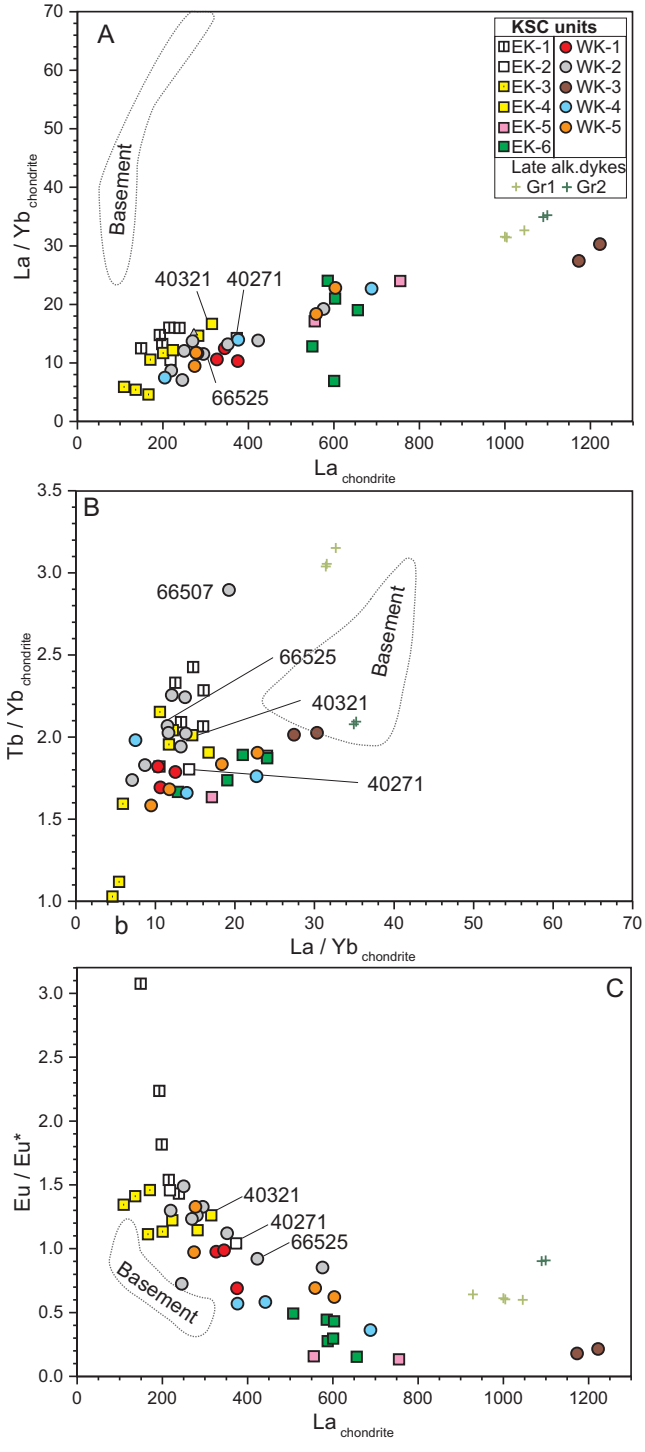

Fig. 7. Chrondrite normalised REE relations in KSC rocks. Approximate melt compositions for EK-2, EK-4 and WK-2 are indicated: 40271, 40321 and 66525, respectively. See text for discussion.

Although the KSC as a whole displays part of a Thingmuli-like FeO^{total} variation (Fig. 4C) proposed to be typical of the liquid line of descent of a tholeiitic magma (Carmichael 1964; Charreteur *et al.* 2013), contents of total alkalis in Kærven syenites and quartz syenites are higher than seen in Icelandic rocks of similar silica range, and the KSC is depleted in CaO and Sr and enriched in K_2O relative to compositions found in Iceland.

EK-1 and EK-2 quartz syenites *s.l.*

The heterogeneous EK-1 and EK-2 intrusions include some of the relatively low-SiO_2 (59 wt%) and high-MgO/FeO^{total} (0.32) rocks at Kærven. Their wide range of silica (59.4–68.0 wt% SiO_2) correlates negatively with TiO_2, Al_2O_3, FeO^{total}, MgO, CaO and P_2O_5 (Fig. 4). The quartz syenites plot on distinctly higher Al_2O_3 and lower FeO^{total} and MnO trends than other Kærven rocks, and in particular higher MgO and P_2O_5, as well as lower K_2O, distinguish EK-1 and EK-2 rocks from the quartz alkali feldspar syenite units with relatively low SiO_2 (WK-2, EK-3 and EK-4).

On the basis of trace element characteristics (see below) we have recognised two subgroups of quartz syenites, EK-1 and EK-2, which are barely differentiated using major element criteria and appear in the field to be one intrusive phase. EK-1 quartz syenites occur close to the contact with the Kærven gabbro and adjoining Archaean basement and span the entire SiO_2 range of Kærven quartz syenites. The remaining part of the quartz syenites are referred to as unit EK-2, which has a more restricted SiO_2 range (61.6–65.1 wt% SiO_2) and tends to have slightly lower amounts of Al_2O_3 and slightly higher FeO^{total} than rocks from the EK-1 unit (Fig. 4). It is argued below that EK-1 quartz syenites comprise both granitic basement-contaminated rocks and rocks influenced by a relatively primitive component. The EK-1–basement relationship is illustrated by the distinctly peraluminous sample 66504, that plots close to the basement field in most variation diagrams.

EK-1 quartz syenites have varied and occasionally very high Ba (1120–5420 ppm) and Sr contents (96–440 ppm) (Fig. 5). EK-2 quartz syenites attain lower enrichments of these elements (1490–3430 ppm Ba and 80–232 ppm Sr). Neither unit shows correlations of these elements with SiO_2, nor positive inter-element correlations such as characterise the main Kærven trend. The variations of Sc and V in the quartz syenites likewise fall outside the main Kærven trend.

Three low-SiO_2 EK-1 quartz syenites have very high V abundances (60–90 ppm) while the remaining samples have 5–12 ppm V. Except for Rb contents, which span a similar range (~30–80 ppm) in the quartz syenite groups, EK-1 quartz syenites typically have half the amounts of Nb, Zr, Y and light REE (LREE) than those of the EK-2 group and also have low Ta and Th. EK-1 quartz syenites are the only Kærven rocks that display a basement-like trough for Nb–Ta in the multielement diagram (Fig. 6E). Both EK-1 and EK-2 units have pronounced Pb peaks. EK-1 has overall more fractionated REEs (La/Yb_{cho} = 12.5–16.0) than EK-2 (La/Yb_{cho} = 10.5–14.2). Both units have either positive or no Eu anomalies (Eu/Eu* = 1.04–3.07; Fig. 7).

WK-2 syenite

Together with EK-1 and EK-2, WK-2 has relatively low SiO_2 (~60–63.5 wt%) and high MgO/FeO^{total} (0.1–0.2). WK-2 syenites display major element trends qualitatively similar to EK-1 and EK-2. However, the low Al_2O_3 and high FeO^{total} of WK-2 syenites clearly set these apart from the KSC quartz syenites (Fig. 4).

WK-2 defines the end of the main Kærven trend with high Ba (2700 ppm), Sr (200 ppm), V (34 ppm) and Sc (28 ppm) (Fig. 5). These elements are negatively correlated with SiO_2. Rb correlates positively with SiO_2. Concentrations of Nb, Zr, Y, Th and LREE increase with SiO_2 in one group of WK-2 syenites whereas a second group, located at the high-SiO_2 end of the WK-2 variation, has markedly lower concentrations of these elements. For example, sample 66525 at 63.6 % SiO_2 has 89 ppm Nb whereas sample 85539 at similar SiO_2 has 50 ppm Nb, and Y contents are 59 and 39 ppm, respectively. WK-2 syenites have a range of positive Ba anomalies of 150–350 times primitive mantle (Fig. 6A) and significant negative Sr anomalies. Nb and elements to the right of Nd are higher in WK-2 relative to the syenites in units EK-3 and EK-4 (see below).

Excluding the outlying sample 66571, WK-2 syenites have less fractionated REE contents than the quartz syenites ($[La/Yb]_{cho}$ 7.1–13.8) and range from negative to positive Eu-anomalies (Eu/Eu* = 0.73–1.47) (Fig. 7).

EK-3 and EK-4 quartz alkali feldspar syenites

These syenites have a narrow range of SiO_2 (*c.* 64–66.5 wt%), extending from the high end of WK-2 rocks. In Harker diagrams (Fig. 4), EK-3 and EK-4 syenites tend to plot in isolation and only occasionally (for TiO_2 and FeO^{total}) along the main trend of Kærven rocks. The exception to this is sample 66554, which in most diagrams plots with WK-2 syenites.

The subdivision into EK-3 and EK-4 is based on MnO, MgO, and K_2O contents. EK-3 has distinctly low MgO and MgO/FeO^{total} (0.03–0.05) and high K_2O and MnO compared to EK-4. The variation of Al_2O_3 appears unsystematic in EK-3, whereas EK-4 seems to define a positive Al_2O_3 correlation with SiO_2. Although WK-2 and EK-3/EK-4 syenites in several Harker diagrams converge at SiO_2 ~64 wt%, the latter two units have lower TiO_2, CaO, MgO, and P_2O_5 at this level of SiO_2.

With relatively low Ba and Sr contents for their SiO_2, EK-3 quartz alkali feldspar syenites (and WK-3, see below) fall below the overall Kærven trend. Furthermore, contrary to the overall Kærven trend, EK-3 and EK-4 syenites tend to show increasing Ba and Sr with increasing SiO_2. As a result, the positive Ba–Sr relationship in these syenites is subparallel to that of the common Kærven trend but displaced towards higher Ba (Fig. 8). Sc levels in EK-3 and EK-4 are 11–23 ppm and similar to WK-2 syenites, while V concentrations in EK-3 and EK-4 are much lower (≤ 6 ppm) than in WK-2 syenites (9–34 ppm) and furthermore, by contrast, positively correlated with SiO_2. The abundances of Rb, Nb, Zr and Y are lower than in the main Kærven sequence, and systematic trends are not pronounced in these groups except for a positive Rb–SiO_2 relationship in EK-3. Although low concentrations of HFSE (High Field Strength Elements) and LREE are typical of EK-3 syenites (Nb~35 ppm, Zr~61 ppm, Y ~23 ppm, La ~25 ppm, Ce~47 ppm), the actual concentration ranges are similar in EK-3 and EK-4. EK-4 syenites display positive Ba anomalies (Fig. 6C) that are not mirrored by the EK-3 unit. Both units have positive Pb and K anomalies. EK-4 syenites are generally richer in the elements to the right of Nd than EK-3 syenites (Fig. 6C). Rocks of both units have positive Eu anomalies in the range 1.14–1.34. EK-4 syenites (La_{cho} = 183–315 and La/Yb_{cho} = 12.1–16.7) are enriched in REE and have more fractionated REE patterns than EK-3 (La_{cho} = 107–200, La/Yb_{cho} = 5.9–11.7) (Fig. 7).

EK-5, EK-6, WK-1, WK-3, WK-4 and WK-5 alkali feldspar granites

WK-1 and WK-5 alkali feldspar granites have similar intermediate SiO_2 levels of 66–68 wt% and 65.5–67.5 wt%, respectively, and MgO/FeO^{total} in the range 0.05–0.15. Major element trends in these bodies are similar and form part of the main Kærven trend (decreasing TiO_2, FeO^{total}, MnO and CaO, increasing Al_2O_3 and K_2O with increasing SiO_2). WK-1 granites, however, are recognised by distinctly higher TiO_2 and FeO^{total} and lower Al_2O_3 than WK-5, and the decrease in MgO with increasing SiO_2 is less marked (Fig. 4).

Alkali feldspar granites from EK-5, EK-6, WK-3 and WK-4 represent the high-SiO_2 end (~68–74 wt%) of Kærven magmatism and display coherent and

overlapping geochemical trends of systematically decreasing amounts of other major elements with increasing SiO_2. In detail, the western WK-3 granites have compositions identical to the low-SiO_2 portion of the eastern EK-6 granites. However, trace element characteristics (see below) show that WK-3 and EK-6 granites are not similar. In the EK-6 unit, TiO_2, FeO^{total}, CaO, Na_2O, K_2O and P_2O_5 display ill-defined trends (Fig. 4). WK-4 granites range to higher SiO_2 and tend to be higher in Na_2O and lower in K_2O than the otherwise comparable EK-6 granites.

With the exception of the WK-3 granite, the Kærven granites display a systematic decrease of Ba and Sr contents with increasing SiO_2. Unit WK-3 has much lower Ba (~300 ppm) and Sr (~20 ppm) at similar SiO_2 than the other granites. In comparison, EK-6 granites with comparable SiO_2 have ~800 ppm Ba and ~70 ppm Sr. Nevertheless, due to sympathetic variation of Sr and Ba in WK-3, this unit plots along the common Kærven trend in a Ba vs. Sr diagram (Fig. 8D). The variation of Sc in the Kærven granites displays a pronounced kink around 69 % SiO_2, separating the EK-5, EK-6 and WK-4 units from the remaining granites. Positive Ba anomalies (Fig. 6) are characteristic for the least evolved alkali feldspar granites (WK-1, WK-5), and the multi-element diagrams for these units are very similar to those for the less evolved WK-2 syenites, both with regard to spikes and troughs and to the relative abundance of elements. Compared to this group, the more evolved granites EK-5, EK-6, WK-3, and WK-4 have lows for Ba, higher positions of the Th–U and La–Ce parts, negative Pb, a large negative

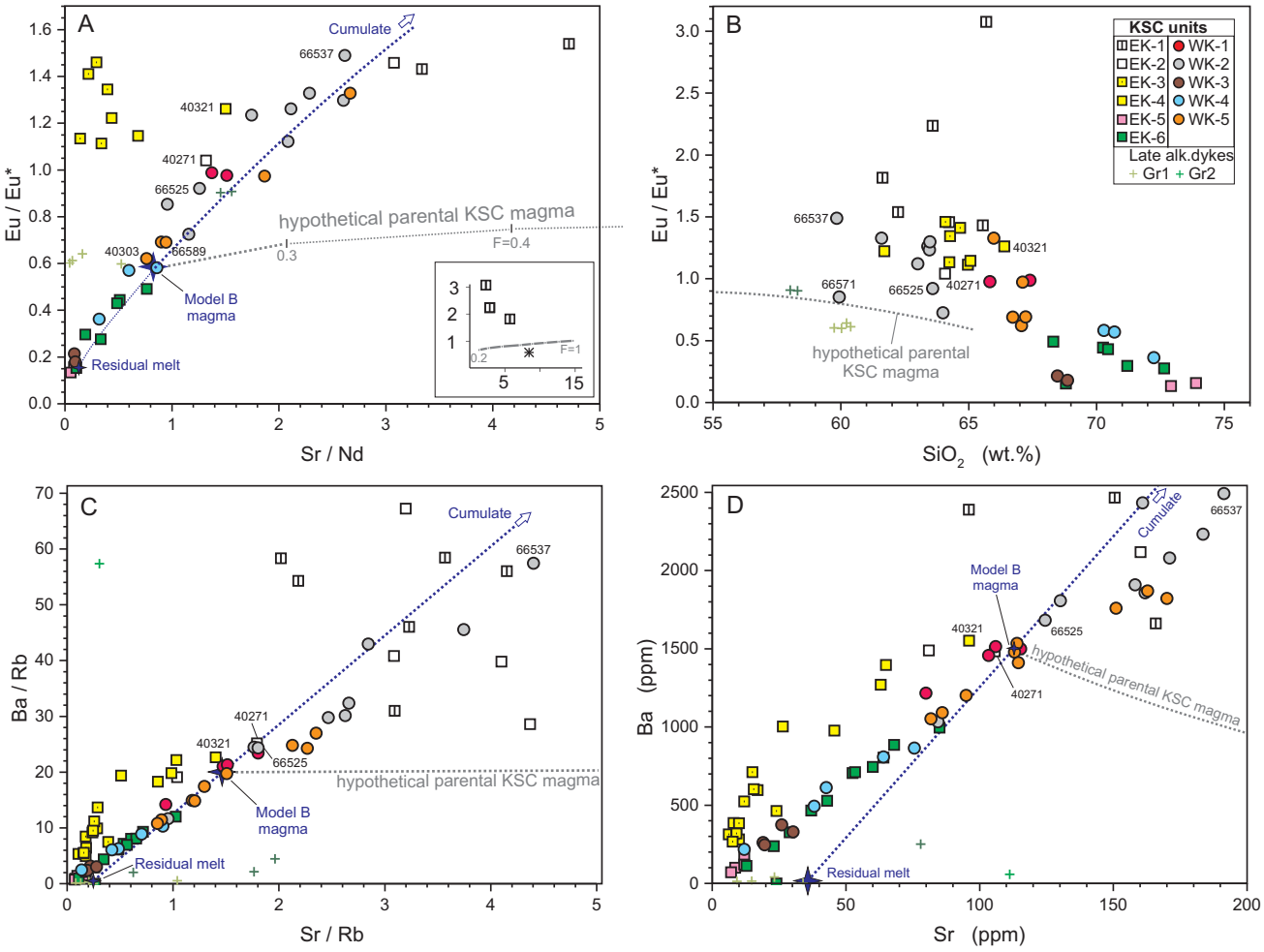

Fig. 8. KSC rocks and the evolution of the hypothetical parental KSC magma plotted in diagrams sensitive to plagioclase fractionation and alkali feldspar accumulation. Shown are KSC sample numbers mentioned in the text. Blue dotted curves in A, C and D represent the compositions of mixtures of modelled residual WK-2 melt and cumulate crystallised from the originally emplaced WK-2 magma. Grey dotted curves illustrate the tentative evolution of a basaltic magma to a compostition emplaced at KSC, e.g. the WK-2 magma; F = fraction of remaining melt. Blue star at end of grey curves is Model B magma of Table 4. Blue star marked Residual melt is a composition modelled for the formation of WK-2. Inset in A shows highly accumulative rocks of EK-1 and an evolving hypothetical Kærven magma with Sr/Nd = 15 typical for oceanic mantle melts (Hofmann 2003). See text for details.

Sr anomaly and higher abundances of elements to the right of Nd. The alkali feldspar granite units have high LREE abundances (La_{cho} = 192–1222) and distinctly fractionated REE patterns (La/Yb_{cho} = 6.9–30.3). Negative Eu anomalies (0.13–0.44) are significant only in EK-5 and EK-6 granites (Figs. 6, 7).

Dykes in the Kærven area

The late green dykes from the Kærven area are peralkaline and silica undersaturated and straddle the trachyte/phonolite boundary in the TAS diagram (Fig. 4O). The dykes have compositions clearly distinct from the main Kærven rocks and combine low SiO_2 (58.0–61.1 wt%) with low CaO (0.8–0.9 wt%) and high amounts of alkalis, and are intermediate between the KAI foyaites and main pulaskites for these elements (Fig. 4F, O). Group 1 consists mainly of trachytes with higher TiO_2, Al_2O_3, FeO^{total}, MnO, MgO, K_2O, and P_2O_5 than Group 2, which mainly comprises phonolites. Both groups stand out with large Nb and Ta peaks of magnitudes not seen elsewhere in the KSC (Figs. 4–6), and they have significant and deeper Ba troughs than Kærven alkali feldspar granites. While Rb, Zr, and Th contents tend to be highest in Group 2, Group 1 has maximum abundances of Y. The late dykes consistently display Eu anomalies in the range 0.60–0.90.

The combination of relatively low SiO_2 and high Nb (243–314 ppm), Zr (790–957 ppm), Th (16–28 ppm), Rb (111–138 ppm) and LREE (200–250 ppm La) is diagnostic for the late peralkaline dykes and quite outside the range of compositions in the KSC. The enrichments in LREE and Nb of the late dykes are even higher than in the KAI where the foyaites reach 73–173 ppm La and 34–117 ppm Nb (Riishuus *et al.* 2008). In this respect the late dykes are not intermediate between KAI foyaites and main pulaskites.

The green dykes at KSC are significantly lower in SiO_2 and are more alkaline than the green peralkaline rhyolite dykes from the Skærgaard peninsula described by Brooks & Rucklidge (1976). Among erratic blocks collected on the Skærgaard peninsula and judged to originate from the interior of Kangerlussuaq, Brooks & Rucklidge (1974) recognised a common variety of green peralkaline phonolites. These authors gave a single analysis (major elements) which is much more silica undersaturated than the green KSC dykes. As it is also less evolved, it is questionable if the Kærven area hosts the original outcrop of the erratic blocks of green phonolites at Skærgaard. Green dykes reported by Bird *et al.* (1985) and Rose & Bird (1994) from the Miki Fjord area do not owe their colour to aegirine but to extensive calcium metasomatism which has stabilised prehnite, epidote and other metasomatic minerals in the dykes. Thus, the 'green dykes' should not be treated as one group with a common petrogenesis, and we will limit our discussion to those from the KSC.

Basement gneisses

During field work, distinction was attempted between the Archaean basement gneisses (Bridgwater *et al.* 1978) and remobilised basement, which is usually recognised by its sugary texture in outcrops. However, major element data of the granodioritic or tonalitic to granitic gneisses do not distinguish between these textural basement types. As a group, the basement has high SiO_2 corresponding to the EK-5 and EK-6 range, and there are compositional overlaps between basement and these KSC units for Na_2O and P_2O_5. However, TiO_2, FeO^{total}, MnO and K_2O are distinctly higher in the Kærven intrusives and Al_2O_3, MgO and CaO are lower than in any of the basement rocks.

Basement rocks are characterised by a combination of high Sr (mostly > 200 ppm), high Sr/Nd (mostly > 22) and high SiO_2, a geochemical feature unlike any Kærven units (Supplementary data file 1). The basement rocks are characterised by extremely low concentrations of a number of elements (Zr < 190 ppm, Nb < 8 ppm and LREE (La < 40 ppm and Ce < 60 ppm)). Multi-element diagrams (Fig. 6J) show significant troughs for U and for Nb–Ta and well developed peaks for Pb. Both positive and negative Ba-anomalies are seen.

Local basement rocks tend to have lower concentrations of REE than the Kærven syenite and granite units, e.g. La_{cho} = 51–273, and Eu anomalies range from slightly negative to slightly positive (Eu/Eu^* = 0.7–1.2) (Fig. 7, Supplementary data file 1).

Comparison with the Kangerlussuaq Alkaline Intrusion and the Astrophyllite Bay Complex

In addition to the differences between KAI and KSC major elements already mentioned, Kærven rocks have significant overlaps in terms of Ba and Sr abundances with the rocks from KAI. Like Kærven, four of five established units in the KAI (Wager & Brown 1968), foyaite, transitional pulaskite, nordmarkite and quartz nordmarkite have individually decreasing Ba with increasing SiO_2 (Riishuus *et al.* 2008). However, the intermediate-SiO_2 main pulaskite unit has increasing Ba and Sr with increasing SiO_2, similar to Kærven EK-3 quartz alkali feldspar syenites, also with intermediate SiO_2 contents. High Ba contents in Kærven quartz syenite units EK-1 and EK-2 (up to 5400 ppm Ba) and WK-2 syenites (~2700 ppm Ba) are unique for the KSC, as KAI nordmarkites peak around 2000 ppm

Ba. High Sr (up to 850 ppm) is characteristic for some KAI foyaites while the most Sr-rich Kærven unit, EK-1 quartz syenite, has a maximum of 440 ppm Sr.

The KAI is generally more enriched in LIL (Large Ion Lithophile) and HFS elements than the KSC. Thus, abundances in the KSC are generally equivalent to the lower levels observed in KAI. For example, the Zr range is 250–1650 ppm in KAI nordmarkites, against 60–1170 ppm Zr in Kærven. Also the typically less incompatible element Y shows a similar difference with 13–67 ppm in KSC rocks and 38–102 ppm in KAI nordmarkites. These many differences of major and trace elements between KSC and KAI clearly demonstrate a contrasting magmatic evolution of the two complexes.

ABC syenites, excluding the one considered contaminated by 90 % crust by Riishuus *et al.* (2005), have much higher LREE, e.g. La = 208–459 ppm, and Zr = 2006–2252 ppm, than any KSC rock with comparable silica (these ABC rocks have a narrow range of 62.5–63.8 wt% SiO_2). KSC sample 66525 has 99 ppm La whereas other rocks with SiO_2 = 62–66 wt% range to 25 ppm La, and Zr displays variation from 600 ppm to much lower values (Fig. 5). Zr/Nb = 39–50 in ABC syenites, much higher than the 1–8 (average 4) in KSC rocks in this silica range, excluding EK-1 which ranges to 14. Thus, the ABC syenites must have had different parental magmas and evolved to very different rocks than found in the KSC.

Discussion

Compared to the previous interpretation of the intrusive events that formed the KSC (Holm & Prægel 1988a; Holm *et al.* 1991) the subsequent field work and geochemical investigations have allowed us to recognise additional intrusive units and offer a more elaborate petrogenetic interpretation of the complex.

Age of the Kærven Syenite Complex

Field relations show that the KSC was emplaced after the Kærven gabbro and before the quartz nordmarkites of the KAI. However, the sequence of intrusion of the eleven distinct units of the KSC is related neither to their geographical position nor to their magmatic evolution (SiO_2). This is a revision of our previous interpretation (Holm *et al.* 1990; Holm *et al.* 1991).

Recent U-Pb zircon age determinations of six units of the KSC by Thórarinsson *et al.* (2016) yielded concordant and overlapping ages between *c.* 53.3 and 53.5 Ma, indicating that the dated KSC units were emplaced within a short time span shortly after the Kærven gabbro, which is dated to 55–53 Ma (Holm *et al.* 2006; Tegner *et al.* 2008). Most available age determinations of the KAI have considerable uncertainties that do not allow elucidation of the time interval between the emplacement of the KSC and the nordmarkites of the KAI, which field relations demonstrate to be younger. However, as Thórarinsson *et al.* (2016), we consider that an Ar-Ar age of 50.8 ± 1.1 (2σ) Ma for the pulaskite unit by Tegner *et al.* (2008) represents a robust determination. In summary, based on the existing age constraints, the KAI may have formed 2–4 Ma later than the KSC.

A multiple ring dyke origin of the KSC was suggested above. The shape of the contact between KSC and KAI and of the outer contact of KAI north and south of KSC suggest that KAI was also formed as a ring dyke complex. This is supported by the above-mentioned contact between nordmarkite and transitional pulaskite, which suggests that the nordmarkite is a ring dyke. In such a scenario, the age span for the formation of nordmarkite, transitional pulaskite and pulaskite is also up to 2–4 Ma (Holm 1990; Tegner *et al.* 2008; Thòrarinsson *et al.* 2016) when allowing for analytical uncertainty in the age determinations.

The late alkaline dykes are younger than at least the nordmarkite of the KAI and are probably related to the very silica undersaturated foyaites of KAI.

Overall evolution of the magmas of the Kærven Syenite Complex

The composition of the KSC rocks show an overall decrease of TiO_2, FeO^{total}, MnO, MgO, CaO, P_2O_5, Sc, and V with increasing silica (Fig. 4A, C–F, I and Fig. 5K, L), similar to what would be expected from an intermediate subalkaline magma evolving to a rhyolitic low-temperature end product by fractional crystallisation. However, the relatively large range of concentrations of several major and trace elements (e.g. FeO^{total}, MgO, P_2O_5, Sr, and Ba) at any silica level, and, generally, the lack of smoothly curved coherent trends encompassing all mapped units of the KSC demonstrate a strong deviation from one liquid line of descent, as expected for plutonic rocks generated at least in part by accumulation of the crystallising minerals during magmatic evolution.

Magma mixing involving two end-members for the entire suite of rocks is ruled out because of the significant kink in all major element Harker diagrams at SiO_2 = 68 wt% (Fig. 4). We do not, however, rule out that various mixing processes could have taken place within the magmas of the individual intrusive units, and emphasise the presence of linear trends for some of the KSC rocks.

Each intrusive unit has a limited compositional variation compared to the total range of KSC. This indicates that the emplaced magmas largely evolved before being intruded at Kærven, and that within-unit variation either reflects withdrawal of compositionally zoned magma from chambers at depth or post-emplacement processes, or both. The lack of a general temporal progression in the compositional evolution suggests that more than one magma must have been involved in the petrogenesis of the Kærven rocks. This is additional evidence that much of the evolution of the KSC magmas took place in one or more precursor magma chambers at deeper levels. The geochemical variation within KSC units was likely caused by a combination of several processes: (1) fractional crystallisation in the local magma chamber of each intrusive unit or in the deeper precursor magma chamber from where a zoned magma rose; (2) accumulation of the crystallising phases; (3) mixing; and (4) late movement of intercumulus melts relative to the cumulus phases.

The comparatively large variations of most elements at any concentration of silica, especially for the more mafic KSC units demonstrate that simple fractional crystallization cannot explain at least part of the geochemical variation within units. In the discussion below, we point to several lines of evidence suggesting that *in situ* accumulation processes within the KSC units were critical in the formation of the Kærven rocks.

Fractional crystallisation and accumulation

Significant plagioclase fractionation is indicated for precursor magmas to the KSC magma as Sr/Nd < 5 in all KSC rocks and thus in melts from which the KSC units crystallised (Primitive Mantle has Sr/Nd = 15, Sun & McDonough 1989). Accordingly, Eu/Eu* would be expected to be somewhat lower than 1.0 in the most primitive of KSC magmas (Fig. 8A). WK-2 rocks 66571, 66525 and 74418 have Eu/Eu* = 0.85, 0.92, and 0.72, respectively, and could exemplify the Eu/Eu* of the initial WK-2 magma, whereas the comparatively low contents of Nb, Zr, Y, and LREE in other WK-2 rocks with Eu/Eu* > 1.20, suggest feldspar accumulation in these rocks. The observed total range of Eu/Eu* = 0.1–3.1 at KSC demonstrates that extensive fractionation as well as accumulation of feldspar took place in the KSC units. The deviation of the syenite units EK-4 and, in particular, EK-3 from the main syenite–granite field, and the discontinuous rock suite of quartz syenite units EK-1 and EK-2 in the Harker diagrams (Fig. 4), are also at odds with a derivation through simple fractional crystallisation of a parental liquid to KSC.

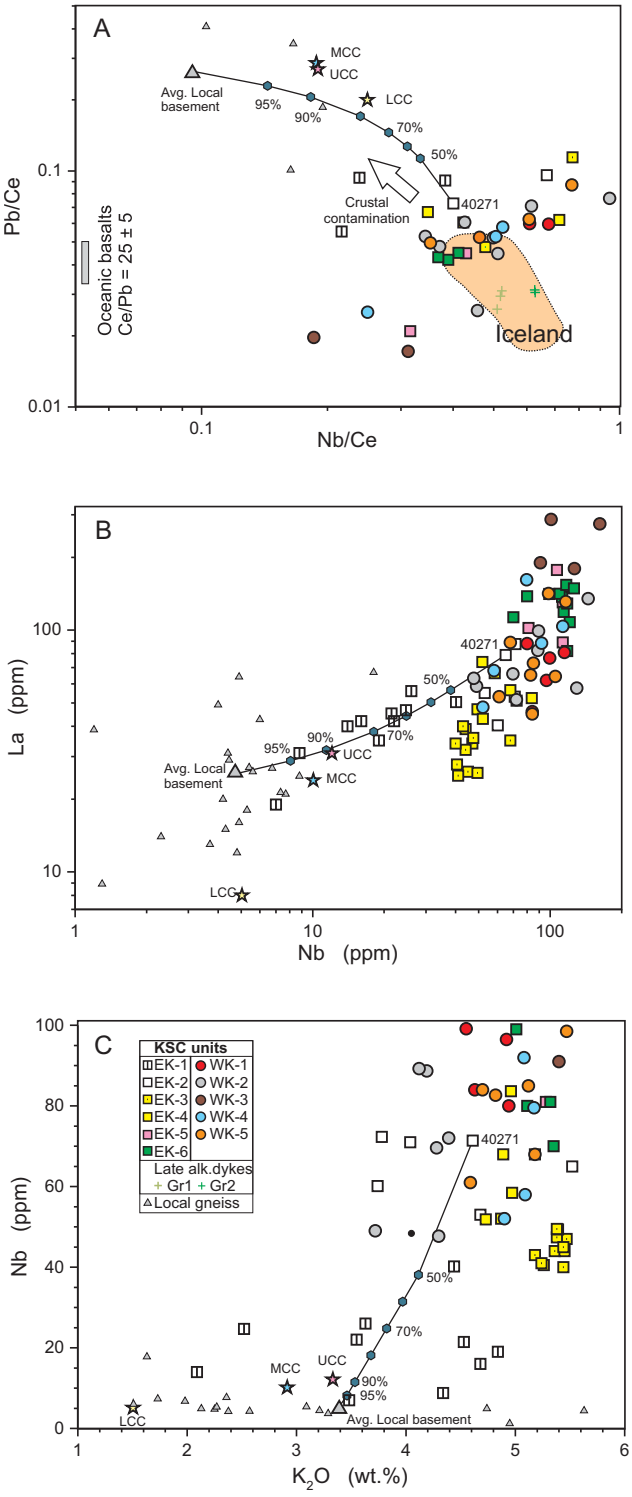

Fig. 9. Modelling of crustal contamination in KSC units EK-1 and EK-2. Shown are KSC, local basement gneisses and average of all local basement gneiss compositions (large grey triangle). UCC, MCC and LCC: upper, middle and lower continental crust, respectively, after Rudnick & Gao (2003). The curve is a mixing curve for EK-1 sample 40271 and average local basement gneiss with indication of fraction of basement. See text for discussion.

Crustal contamination of the magmas

The common occurrence of xenoliths of basement gneisses in EK-1 is evidence for the possible contamination of Kærven magmas. The geochemical effects of this in EK-1 rocks will be discussed separately below. In general, however, most other KSC rocks display little evidence for crustal contamination. Continental crust in general (Rudnick & Gao 2003), and local basement in particular (Supplementary data file 1), are characterised by low Nb/U < 25 and Ce/Pb < 5, in contrast to oceanic basalts. KSC rocks have oceanic Nb/U = 40–100. If these trace elements are considered incompatible in the cumulative phases, the positive correlation of Pb/Ce and Nb/Ce ratios illustrate the limited crustal component in KSC rocks in general (Fig. 9A). Most KSC rocks display a trend overlapping with, but normal to, compositions of Iceland basaltic rocks, and normal to the direction towards both local and global crustal averages (Fig. 9A). The evolved KSC rocks in many other respects do not have large compositional contrasts to the potential contaminants such as the granitic gneisses or their anatectic melts, and therefore a considerable degree of crustal contamination would be required to make significant compositional changes in the magmas from which the KSC rocks crystallised. This, and the geochemical effects of fractionation or accumulation of several accessory phases, especially in the most evolved KSC melts, impede assessment of the likely, but limited, extent of crustal contamination. As an example, the decrease of Nb among the most evolved rocks in EK-5, EK-6 and WK-4 (Fig. 5B) is not necessarily a sign of crustal contamination but related to fractionation of Nb-rich accessory minerals such as titanite and zircon. Alkali feldspar has some affinity for Pb, and therefore a slightly higher Pb/Ce ratio in some EK-3 rocks is likely, at least partly, to be caused by alkali feldspar accumulation, and the trend of KSC may be explained by mixing of melt and various cumulus assemblages including accessory phases such as apatite. Also, in the La vs. Nb diagram (Fig. 9B) the relatively well-defined field of KSC rocks except for EK-1 trends obliquely to the direction of crustal rocks.

In studies of syenitic to granitic rocks of nearby intrusions, large degrees of crustal contamination are suggested mainly based on indications from radiogenic isotopes. For the ABC, a mantle-derived magma was modelled to be contaminated in the lower crust by granulite and subsequently evolved to trachybasalt magma, and another magma was modelled to be contaminated in the upper crust by amphibolite and subsequently evolved to trachyte, which then rose and mixed with local basement gneiss (Riishuus *et al.* 2005). For the KAI, Riishuus *et al.* (2008) proposed that deep-seated alkaline primitive magma assimilated crustal material to become trachytic and emplaced as the outer nordmarkite, and that subsequent batches of magma formed as less contaminated and more evolved alkaline melts in the deep magma chamber before emplacement as the inner KAI units. The discussions of these hypotheses were based on radiogenic isotope data and do not include evidence from incompatible trace elements, which is the basis for our present evaluation of the possible effects of crustal contamination on KSC melts. A comparison of our trace element-based modelling of the KSC with the models of Riishuus *et al.* (2005) and Riishuus *et al.*(2008) awaits radiogenic isotope analysis of representative KSC rocks.

The formation of unit WK-2

A number of geochemical features indicate that mineral accumulation was an important process in the development of the WK-2 and EK-3/EK-4 rocks. WK-2 syenites, except 66571, show a good, linear correlation between several major oxides which reside mainly in mafic minerals: TiO_2, Fe_2O_3, FeO, P_2O_5, CaO, MnO, and MgO (Figs. 4 and 10, Table 3). Such correlations can be generated during melt differentiation or by accumulation of mostly mafic minerals.

An indication of accumulation of clinopyroxene is found in WK-2 (and in EK-3/EK-4), which has up to 27 ppm Sc (Fig. 5K) in rocks with low MgO/FeO^{total} ratios of 0.12–0.14, demonstrating an evolved character of the rock. This Sc level is much higher than in evolved melts that have fractionated considerable amounts of clinopyroxene, as seen among evolved dacites and rhyolites in Iceland (e.g. Jónasson 2007). The rock budget for Sc must be dominated by accumulation of the only likely phase, clinopyroxene, in which Sc is compatible.

Ratios of major oxides can be used for estimates of the composition of the mafic cumulus assemblage (Table 3) because several regression lines pass close to the origin (Fig. 10). The relatively felsic end of the correlations would then be expected to represent less accumulative rocks or even approximations to further evolved melt compositions.

In detail, sample 66571 is not part of the trend of the rest of WK-2 due to its relatively small component of clinopyroxene (low CaO and Sc) and large plagioclase content (high Na_2O). Sample 66505 has *c.* 500 ppm Nb, possibly due to small amounts of niobophyllite or niobokupletskite varieties of astrophyllite (Piilonen *et al.* 2003). Astrophyllite is a common accessory mineral in the silica oversaturated syenites in the Kangerlussuaq area (Brooks & Nielsen 1982) and has been observed in sample 66507. Also the somewhat high Nb in sample 74418 may be caused by trace amounts of this mineral.

Other outlying values of trace elements may also indicate the occasional gain or loss of zircon or titanite in some of the WK-2 rocks (Fig. 5). Anomalies in trace element concentrations therefore appear to be a result of variation in the crystallising and/or accumulating/fractionating mineral assemblage of KSC rocks.

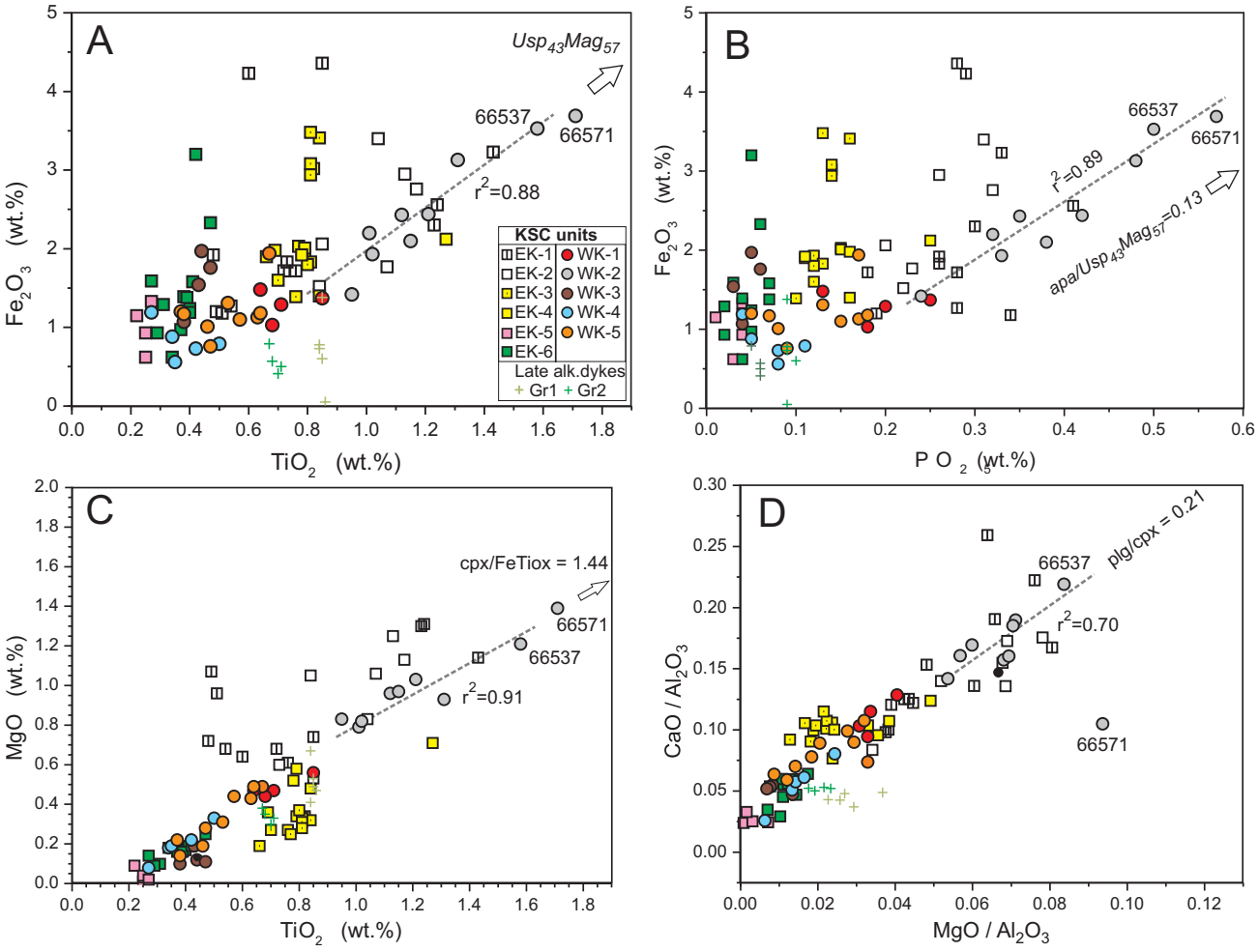

Fig. 10. Model of the formation of KSC unit WK-2. Shown are the linear regressions for WK-2 (without sample 66571) with correlation coefficients, r^2 (grey dashed lines). Mafic end-members for two-component mixing are indicated: FeTi-ox (Ulvöspinel 43 % - Magnetite 57 %); apa: apatite; cpx: clinopyroxene; plg: plagioclase. See Table 3 and text for discussion.

Table 3. Correlations between major oxides of unit WK-2

Compositional parameter		Correl. Coeff.	Straight line parameters§		Indicated mineral	Indicated mineral composition (wt.%)						
Oxide	Oxide	r^2	a	b		TiO_2	Fe_2O_3	FeO	MnO	CaO	MgO	SiO_2
TiO_2	Fe_2O_3	0.88	2.75	-0.842	$Usp_{43}Mag_{57}$	15.06	39.9	45.04				
TiO_2	MnO	0.81	0.104	0.145	$Usp_{43}Mag_{57}$	15.06	39.9	42.75	2.29			
CaO	FeO	0.87	-0.644	0.616	augite Mg#45			18.1	1.1	20.5	8.4	51.3
P_2O_5	Fe_2O_3	0.89	7.27	-0.346	apa/ox = 0.13							
MgO/Al_2O_3	CaO/Al_2O_3	0.70	2.17	0.0284	plg/cpx = 0.21							
TiO_2	MgO	0.91	1.352	-0.1051	cpx/ox = 1.44							

Combined result from correlations: Apa : Plg : Cpx : FeTiox = 4.5 : 10.5 : 50.1 : 34.8 (sum=100)

§ y = ax + b. See Fig. 10.

The samples of WK-2 and EK-3/EK-4 display well defined linear trends in a diagram of 1/Rb vs. K/Rb (Fig. 11A), which suggests two-component mixing to be important for both units. K and Rb are essentially present only in alkali feldspar and in the melt (besides in very minor late crystallised biotite), and $K/Rb_{alkfsp} > K/Rb_{melt}$ due to the relatively low (0.3–0.7) partition coefficient for Rb into alkali feldspar (Philpotts & Schnetzler 1970; Mahood 1981; Bachmann *et al*. 2005). Therefore, the indicated end-member components in both cases are a low-K/Rb melt and a high-K/Rb alkali feldspar-bearing mineral assemblage. Before alkali feldspar began to crystallise in KSC melts, K/Rb in the melts would remain unchanged during fractional crystallisation, and its value would be expected to be inherited from the melt source. If this is assumed to be Primitive Mantle with K/Rb around 394 (Sun & McDonough 1989), it is remarkable that most KSC rocks, and all WK-2 and EK-3/4, have K/Rb above 400, ranging to 979 in WK-2 and 1075 in EK-3. This demonstrates that most KSC rocks contain accumulated alkali feldspar. Only some granitic KSC rocks have ratios below 400 (Fig. 11A), as expected in melts after alkali feldspar fractionation. Alkali feldspar accumulation in WK-2 is also demonstrated by several other key features: low Th/Rb (Fig. 11C) and La/Rb ratios, high to very high Ba (up to 2500 ppm, Fig. 5) and Eu/Eu* up to 1.5 (Figs 7, 8).

If WK-2 rocks represent compositions intermediate between an evolved silicate melt and an accumulation of the liquidus mineral assemblage of this melt, i.e. a classical cumulate rock composed of cumulus phases and trapped liquid (e.g. Wager *et al*. 1960; Wager & Brown 1968), their linear trend of increasing silica and alkalis in Fig. 4O would suggest that alkali feldspar was not a significant part of the cumulus and thus liquidus assemblage. In such a scenario the WK-2 rocks with the lowest inferred cumulus fraction are those with the highest silica. These have Eu/Eu* < 1, and 63–64 wt% SiO_2.

The evidence from somewhat comparable tholeiitic magmas, e.g. the basalt-rhyolite volcanic suites of Ljósufjöll, Iceland (Martin & Sigmarsson 2007; Flude *et al.* 2008) and Boina, East Africa (Barberi *et al*. 1975) suggests that alkali feldspar fractionation is initiated once the melt reaches around 69 % SiO_2. Based on this observation, we conclude that crystallisation of alkali feldspar in the WK-2 magma at emplacement is not indicated.

Also, studies of the system Qz-Ab-Or-An (James & Hamilton 1969) and experimental melting of trachytic rocks (Naney & Swanson 1980; Iezzi *et al*. 2008) suggest that alkali feldspar is a relatively late crystallising phase in sodic subalkaline magmas such as those common in the East Greenland Palaeogene igneous province. Another type of accumulation process is therefore indicated for the high-K/Rb rocks of WK-2 and EK-3/EK-4 that require alkali feldspar accumulation.

Some WK-2 rocks are characterised both by the most mafic mineral assemblages of KSC (up to 30 % mafic minerals), thus indicating crystallisation from relatively unevolved melts, and by a significant component of alkali feldspar, which is typical of very evolved melts. This contrast can be explained by *in situ* fractionation (Langmuir 1989). If the rocks were formed by wall rock crystallisation during conductive cooling (McBirney & Noyes 1979) in a stagnant crystal-melt mixture (Jackson 1961), and if, at some stage of crystallisation, melt was lost from this mush, as explained by Langmuir (1989), the effect would be that the plutonic rock composition would be that of the initial melt less the lost residual melt. The trend of WK-2 rock compositions in Fig. 11A suggests that one relatively well-defined mafic cumulus assemblage is present in the rocks. Well-correlated major elements of WK-2 allow this assemblage to be constrained (Table 3, Fig. 10). The calculated mafic part of the WK-2 cumulus assemblage is clinopyroxene:oxide:plagioclase:apatite = 50:35:11:4.

Fig. 11A also shows that alkali feldspar was added to this mafic mineral assemblage. It therefore appears that an interval of crystallisation is reflected in the WK-2 rocks, during which alkali feldspar started to crystallise from the interstitial liquid. In this scenario the WK-2 rocks are dominated by the crystals formed from a melt evolving to a certain stage, at which the remaining melt was partially lost. With both crystallised and melt components relatively well defined, the important variable for the WK-2 rocks is to what extent the remaining liquid was expelled from the crystal mush. Two quantitative models for this are shown in Figs. 11B, D and F.

Quantitative modelling of the formation of WK-2

The sequence of appearance of liquidus phases in the crystallising KSC magmas based on petrography was discussed by Holm & Prægel (1988a), who found that alkali feldspar invariably crystallised first, followed by a variable sequence of mafic phases and quartz, with early clinopyroxene and olivine, when present. However, cumulus textures remain elusive in KSC, as it was found in general to be the case for intermediate and silicic plutonic rocks by Deering & Bachmann (2010). Because of the uncertainty related to the interpretation of petrographic information, we choose to present two evolution models for the WK-2 melts based on geochemical constraints. Each model includes three steps of crystallisation of the intermediate magma parental to WK-2.

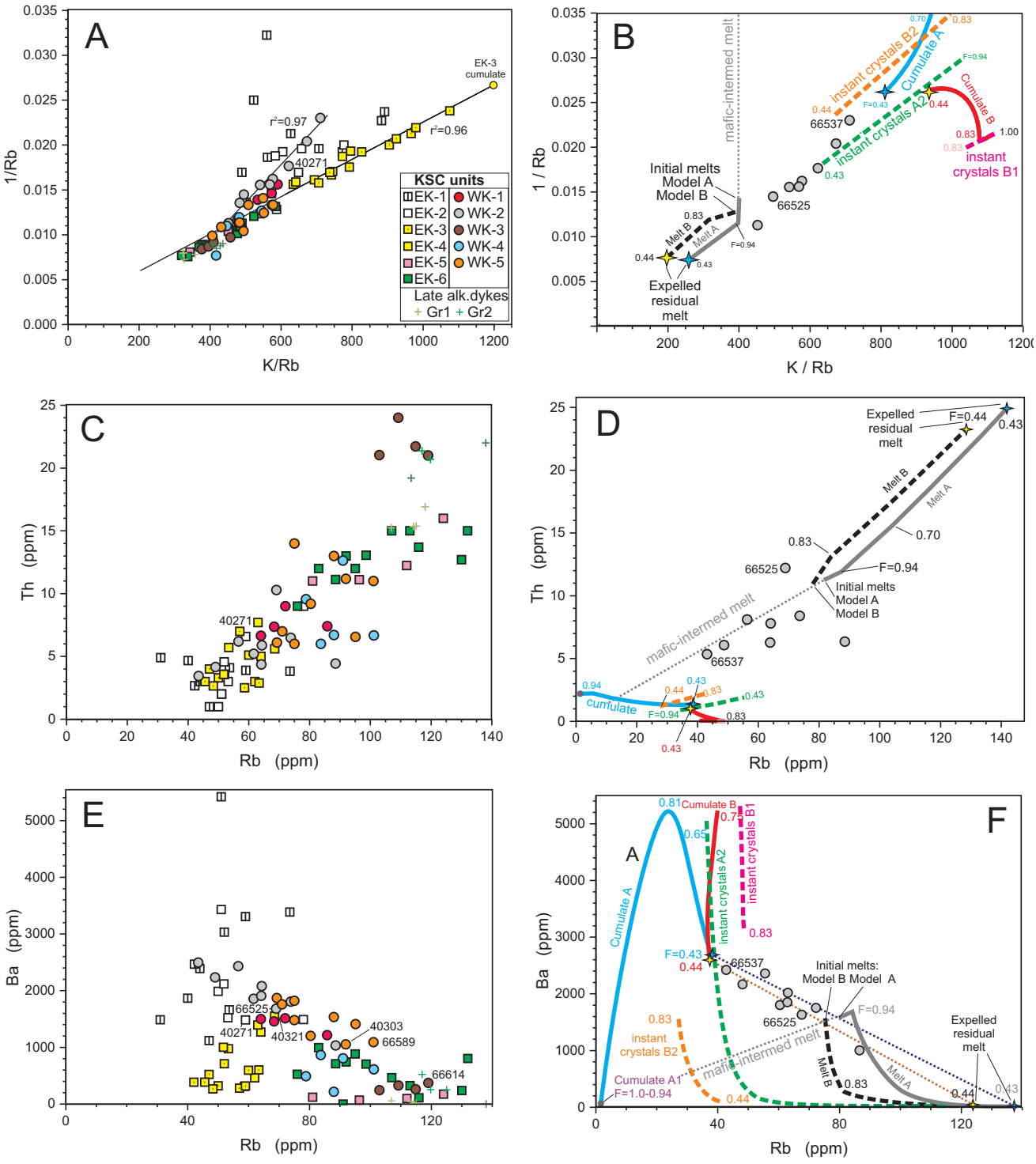

Fig. 11. Crystallisation models for the KSC, see text for explanation and Table 4 for details. Left panels: all KSC samples. Right panels: WK-2 rocks and two crystallisation models. For **B**, **D** and **F**: *Model A*: purple dot (in D and F): diorite cumulate of Stage A1; green dashed curve: alkali feldspar syenite crystallisation as it changes during Stage A2; blue curve: total crystals as the cumulate evolves; grey curve: melt; blue stars: final cumulate and expelled melt, respectively. *Model B*: magenta dashed curve: alkali feldspar crystallisation as it changes during Stage B1; orange dashed curve: alkali feldspar syenite crystallisation as it changes during Stage B2; red curve: total crystals as the cumulate evolves; black dashed curve: melt; yellow stars: final cumulate and expelled melt, respectively. For both models: F: fraction of remaining melt. In **A**: thin black lines are regressions for WK-2 and EK-3/EK-4, respectively.

Model A: First, a dioritic assemblage crystallises, followed by an alkali feldspar syenitic assemblage, and finally residual interstitial melt crystallises.

Model B: First, alkali feldspar crystallises alone, followed by an alkali feldspar syenitic assemblage, and finally the residual interstitial melt crystallises.

Model A would approximate the sequence of crystallisation on the liquid line of descent of the WK-2 magma at a given pressure. Model B assumes the expansion of the alkali feldspar stability field in the granite system due to relatively low water pressure at decreasing pressure (Luth 1969; Becker *et al*. 1998). This would cause a rising intermediate WK-2 melt to develop a relatively high K/Na ratio as plagioclase fractionated at higher pressure, and then experience an interval of crystallisation of solely alkali feldspar after final emplacement at lower pressure, until the melt evolved to cotectic conditions where alkali feldspar precipitated together with mafic minerals and plagioclase. In both models the mafic phases are modelled to have crystallised in the proportions listed in Table 3.

The three stages of our models are illustrated by the variation in Ba and Rb (Fig. 11E–F) which are very compatible and slightly incompatible, respectively, in alkali feldspar, but both incompatible during earlier crystallisation of the melt. We use elements that are compatible in alkali feldspar because this mineral is the dominant phase in all KSC rocks. The starting magma in Model A is of intermediate composition with a dioritic liquidus mineral assemblage that is poor in Ba and Rb (Stage 1). When the melt is retained in a mush composed of melt and crystals of liquidus phases, it is considered to be an intercumulus liquid and will evolve and eventually start crystallising alkali feldspar, which will thereafter dominate the interstitial mineral assemblage (Stage 2) which will be equivalent to alkali feldspar syenite. The effect of the high $K_d(Ba)^{\text{alkali feldspar/melt}}$ for the Stage 2 melt is a marked by a rapid depletion of Ba. Only the first-formed alkali feldspar will be highly enriched in Ba. Thus, Ba will increase from near zero in the dioritic Stage-1 cumulate to maximum concentrations as early-formed alkali feldspar crystallises at the start of Stage 2, and then decrease as the fraction of alkali feldspar syenitic assemblage increases. If the mush melt crystallises completely (as trapped liquid), then the final rock composition will be that of the initial mush. A clear implication of the high Ba of WK-2 rocks is therefore that Ba-depleted melt was expelled at Stage 3 well before complete crystallisation. The quantitative model for the evolution of the WK-2 magma involves 6 % crystallisation at Stage 1 (i.e. remaing melt F = 0.94) and 51 % at Stage 2, leaving 43 % remaining interstitial melt for Stage 3 (F=0.43) (Model A, Table 4). The position of WK-2 rocks along the linear trend in Fig. 11F illustrates the variation of the fraction of interstitial liquid expelled before final crystallisation.

Ba and Rb of the expelled liquid plot on the extension of the line between initial melt and cumulate in Fig. 11F, and the broad linear array of WK-2 rocks indicates an approximately fixed composition of cumulate as well as of remaining interstitial liquid at the stage of expulsion. Moreover, the rather tightly constrained high-K/Rb end-member of WK-2 (Fig. 11B) leaves little room for variation in the amount of crystallisation before the liquid was isolated, and also shows that at the sampled locations the WK-2 melt crystallised approximately to the same degree before expulsion. This supports that the only important variable is the fraction of residual interstitial melt expelled from the solidifying mush. The WK-2 rocks are then composed of near constant proportions of dioritic (Stage 1) and quartz-syenitic (Stage 2) liquidus parageneses and a variable proportion of material crystallised from residual and intercumulus melt (Stage 3).

Among the WK-2 samples, 66525 seems to be least affected by alkali feldspar accumulation or fractionation, having Eu/Eu* = 0.92 and K/Rb near mantle values; furthermore it is situated near the end of the WK-2 trends in Fig. 11B, D and F. The relative enrichment in alkali feldspar for several WK-2 samples is indicated by high K/Rb and low La/Rb and Th/Rb (Fig. 11D). For KSC rocks with Rb < 80 ppm (except 66571), there is a maximum La/Rb around 1.5 and Th/Rb around 0.15, suggesting these to be the values of the parental melt and possibly even the source. These values are intermediate between Primitive Mantle (PM) and Depleted MORB Mantle (DMM). This is in accord with La/Rb = 1.4 for 66525. The overall difference between melt-like sample 66525 and sample 66537 with high K/Rb and low La/Rb is the lower abundances of most incompatible and most compatible elements in the latter (Fig. 6A).

We have also modelled mineral accumulation and residual melt evolution as illustrated by Eu/Eu* vs. Sr/Nd and Ba/Rb vs. Sr/Rb (Fig. 8A, C). With very feldspar-compatible Ba, Sr and Eu as numerators and relatively feldspar-incompatible Nd and Rb as denominators, these ratios are particularly suitable for demonstration of the role of interstitial melt expulsion from a crystal mush in magmas on the verge of onset of alkali feldspar crystallisation. In WK-2 bulk compositions, Eu/Eu* correlates positively with Sr/Nd, as is also the case for Ba/Rb and Sr/Rb, and both Eu/Eu* and Ba/Rb attain high values, clearly indicting accumulation of alkali feldspar.

The composition of the alkali feldspar in the cumulates is important for the modelling and can be inferred from the K/Na ratios (< 2 % biotite or other K-bearing phases, Table 1). With increasing K/Rb, K/

Na in WK-2 rocks trends hyperbolically towards alkali feldspar composition Or_{35} (Supplementary data file 2). For EK-3 rocks, ~Or_{39} is indicated. Based on this and model A melt with 70 ppm Rb, the high-K/Rb component for WK-2 is derived to be composed of alkali feldspar (Or_{35}) and 'others' in the ratio 54:46 (Fig. 11B); 'others' comprise K-free clinopyroxene, plagioclase, FeTi-oxide and apatite, in the proportions indicated in Table 3 and Fig. 10. Late amphibole and biotite are thought to be formed from the residual melt and not to be part of the cumulate assemblage.

Crystallisation in Model B encompasses a slightly less evolved initial melt than in Model A (Fig. 11B, D, F, Table 4). Stage 1 is limited to 17 % alkali feldspar crystallisation to allow Stage 2 to evolve to a composition with Ba, Rb and Th close to the end cumulate composition of Model A, which is approximately attained for F (fraction of remaining melt) = 0.44. Also in Model B the bulk compositions of WK-2 rocks can be explained by the sum of the cumulate and a non-expelled fraction of the residual interstitial melt.

We thus conclude that either of the two models can explain the formation of the WK-2 rocks, with the exception of sample 66571.

Table 4. Parameters for modelling of the formation of unit WK-2

Compositions of melts and cumulates							
	Rb	Ba	Th	1/Rb	K/Rb	Th/Rb	Ba/Rb
	ppm	*ppm*	*ppm*	*ppm^{-1}*			
Model A							
WK-2 initial melt 1	70	1400	10	0.0143	400	0.143	20,0
Stage 1 – 6 % crystallisation							
Gabbro cumulate compos.	0.4	18	2.3	2.5	0	6.5	50
Magma compos. (F=0.94)	74.4	1486	10.5	0.0134	400	0.141	20
Stage 2 – 36 % crystallisation							
AF cumulate							
End cumulate composition	38.2	2782	1.4	0.0262	809	0.054	72.8
Magma compos. (F=0.43)	141.3	19	25	0.0071	247	0.177	0.14
Model B							
WK-2 initial melt 2	77.7	1554	10.9	0.0129	400	0.14	20
Stage 1 – 17 % crystallisation							
AF cumulate at F = 0.83	48.3	7817	0.01	0.0213	1084	0.0019	162
Magma compos. (F=0.83)	83.6	301	13.1	0.012	321	0.156	3.6
Stage 2 – 38 % crystallisation							
AF syenite cumulate							
End cumulate composition	38	2730	1.2	0.0263	937	0.0368	71.8
Magma (F = 0.44)	130	16	23.6	0.0077	194	0.175	0.13

Liquidus phases				**Liquidus mineral assemblage**			
				Model A		**Model B**	
	Partition coefficients			*Stage 1*	*Stage 2*	*Stage 1*	*Stage 2*
	Rb	Ba	Th	Fraction	Fraction	Fraction	Fraction
Alkali feldspar	0.6	10	0.001	0	0.66	1	0.55
Plagioclase	0.04	0.1	0.01	0.33	0	0	0.05
Clinopyroxene	0	0	0.01	0.40	0.19	0	0.23
Magnetite	0	0	0.001	0.23	0.14	0	0.16
Apatite	0	0	5	0.04	0.02	0	0.02

Crystal-liquid relations in the formation of syenite units EK-3 and EK-4

Due to the very high FeO (67 wt%) and MnO (4.5 wt%) in $Fa_{97–99}$ olivines in syenites EK-3 and EK-4 and in granites WK-1 and WK-3 (Holm & Prægel 1988a), their fractionation from the host rocks would tend to drive the residual melt towards lower FeO^{total} and MnO and higher SiO_2. However, the opposite is the case for EK-3 (Fig. 4C, D, E, M and N), which is instead consistent with accumulation of fayalite, and this also explains the position of the EK-3 rocks at relatively low MgO/ FeO^{total} in Fig. 4M. By contrast, the notable amounts of euhedral crystals of fayalite in WK-1 and WK-3 (Table 1) do not seem to be accumulative, as these units have higher ratios of MgO/ FeO^{total} close to those of the KSC rocks without olivine.

Many trace elements display large variations in these units and in EK-3 range to low values of 53 ppm Zr and 25 ppm La (Fig. 5C, G), which are only a fraction of the concentrations found in most KSC rocks and demonstrate the dominance of cumulus minerals virtually free of Zr and La. The strongly cumulative nature of EK-3 and EK-4 is also demonstrated in a Th vs. Rb diagram (Fig. 11C) in comparison with WK-2. The positive Eu anomalies (Fig. 8A) as well as low Rb (Fig. 5D) of EK-3 and EK-4 enforce that they are enriched in cumulative alkali feldspar. Importantly, the low Ba and Sr (particularly in EK-3) are an indication that the alkali feldspar formed from very evolved magma that had previously been depleted in Ba and Sr by fractionation of considerable amounts of alkali feldspar (Fig. 5E, F). This is in stark contrast to the accumulation of early-formed alkali feldspar in WK-2.

The very good linear correlation between K/Rb and 1/Rb for EK-3 and EK-4 (r^2=0.96, Fig. 11A) strongly indicates that two well-defined main components account for K and Rb in these rocks, and the high-K/Rb component comprises alkali feldspar Or_{39} and mafics in the proportion 79:21. The mafic part of the cumulate can be constrained further using Mn/Rb vs. K/Rb, and this calculation yields 10 % fayalite with 4.4 wt% MnO, as these units have no FeTi oxides. Because of high $K_d(Sc)^{cpx/melt}$, which may reach >100 in rhyolites (Sisson 1991), the correlation of Sc with CaO (Supplementary data file 2) can be explained by less than 2 % cumulus clinopyroxene. Assuming a Zr-free cumulate and that EK-4 sample 40321 represents a melt composition (as it is the sample with the highest Zr/K ratio, Supplementary data file 2), 11 % remaining melt is calculated for sample 40332 (Supplementary data file 2). The range of incompatible elements in EK-3 and EK-4 is illustrated in Fig. 6C, D.

With around 300 ppm Ba in several EK-3 rocks with 80–90 % cumulus minerals as indicated by their low Th, La, and Zr contents, the alkali feldspar of these cumulates will have < 400 ppm Ba. The melts in equilibrium with this alkali feldspar would have < 50 ppm Ba (using $K_d(Ba)^{AF/melt}$ = 10, Icenhower & London 1996). There is a large discrepancy between such melt and the 1500 ppm Ba of EK-4 rock 40321. This we interpret to demonstrate that the alkali feldspar-fayalite cumulate part of EK-3 and EK-4 had its residual interstitial liquid replaced by magma less evolved than the WK-2 magma. Thus, EK-3 and EK-4 rocks may represent mixtures of cumulus minerals and two melt components, one being the remaining very evolved melt (i.e. undefined EK-3 melt) and the other a less evolved melt replacing it (EK-4 magma). The variation in Rb abundances among EK-3 rocks may be caused by variable Rb enrichment levels in the interstitial melt prior to addition or replacement by the assumed EK-4 melt.

Because K/Rb must be higher in the cumulate assemblage than in any EK-3 rock, we use K/Rb = 1200 to calculate Rb = 37 ppm in a model cumulate (Fig. 11A). For the associated melt, which, as derived above in Supplementary data file 2, crystallised alkali feldspar with composition Or_{39}, a value of 79 ppm Rb is indicated, which is at the low end of the most silicic low Ba, high Rb KSC rocks (Fig. 5), and thus lower than the most silicic melts. We note that our modelled residual WK-2 melt has Rb > 100 ppm as Ba decreases below 400 ppm. This indicates that the EK-3 magma deviated significantly from the WK-2 magma.

Feldspar accumulation and mixing with anatectic basement in the formation of syenite units EK-1 and EK-2

The poorly defined compositional trends displayed by rocks from units EK-1 and EK-2 (Fig. 4) negate the possibility that simple fractional crystallisation explains the variation of rocks of the two units. Some aspects of EK-1 and EK-2, e.g. Eu/Eu* = 1.4–3.1, Ba =1120–5420 ppm, and K/Rb = 900 at moderate Rb = 40–60 ppm, are akin to WK-2 and are ascribed to accumulation of alkali feldspar and loss of evolved residual melt. We therefore propose that the crystallisation history for EK-1 and EK-2 is similar to WK-2. High Sr and Sr/Ba in samples 66453, 66501 and 66580 indicate a significant amount of accumulated plagioclase, and these rocks deviate most from any envisaged cumulate–lost liquid mixing line in Fig. 8C. Among EK-1 and EK-2 rocks, we identify dyke rock 40271 with its relatively low K/Rb and Ba and high Rb as the closest to a model melt composition in Fig. 11. The variation of incompatible element patterns in these units is displayed in Fig. 6E, F.

The unequivocal field evidence for at least mingling with local basement and gabbro lithologies in EK-1 is

supported by geochemical variations readily explained by addition of local crustal rocks (or melts thereof) to KSC magmas such as approximated by sample 40271. Low Nb < 30 ppm and Nb/La = 0.3–0.5 clearly separate EK-1 rocks from the rest of KSC (Fig. 9B). Simple mixing calculations based on Nb and La indicate 50–95 % average local crust in the samples. EK-1 seems to represent a full range from basement gneiss to intruded magma. The obliqueness of the EK-1 trend to the trend of other KSC rocks in Fig. 9B emphasises the limited role of crustal contamination in the latter. In a diagram of Nb vs. K_2O (Fig. 9C) very different levels of potassium are found in EK-1 samples with a very high basement component, i.e. with very low Nb. We consider this to reflect that the EK-1 magma assimilated a cross section of the crustal lithologies present around Kærven. Together with the lack of significant contamination in most other KSC rocks this probably demonstrates that substantial contamination was limited to the early stage of KSC development when the EK-1 magma was emplaced. The incorporated basement rocks seem to range from whole rock tonalitic gneiss with 68–69 wt% SiO_2 and 1–2 wt% K_2O to anatectic granitic melts much richer in SiO_2 and K_2O, as exemplified by basement samples with 73–75 wt% SiO_2 and 5–6 wt% K_2O. For EK-1 rocks with SiO_2 > 63 wt%, the broad negative correlations of Nb (Fig. 5B) and the LREE with silica demonstrate that assimilation-fractional crystallisation (AFC) is unable to fully explain the variation as these elements are expected to be incompatible.

In the group of low-SiO_2 EK-1 samples, a few rocks stand out with comparatively high V (61–90 ppm). This may be caused by the relatively primitive character of the basement, as shown by its relatively high Mg# (up to 55) despite high SiO_2, or by mixing with mafic material of the Kærven Gabbro. Support for mixing as the hypothesis for contamination is evident from specific EK-1 samples shown above to be particularly contaminated and offset in Fig. 4J from the trend of most KSC rocks towards both high SiO_2 and high Mg#.

EK-2 is considered to have formed from a magma similar to the EK-1 magma but without much contamination and was possibly emplaced separately.

Formation of the most evolved granitic units

The granitic units of the KSC (EK-5, EK-6, WK-1, WK-3, WK-4, WK-5) show the overall effects of feldspar fractionation: decreasing Eu/Eu* and Sr/Nd (Fig. 8A), as well as decreasing Sr and Eu with increasing SiO_2 (Fig. 5E and H). We divide the most evolved units of the KSC into two groups: The first of these comprises units WK-1 and WK-5, whose geochemical characteristics are comparable to the approximate melt compositions inferred above for units EK-2, EK-4 and WK-2. WK-1 and WK-5 have increasing alkalis and decreasing TiO_2, FeO^{total}, MnO, MgO, CaO and P_2O_5 with increasing silica (Fig. 4), and their most silica-poor members have Ba, Sr, Zr, Th and Rb not much different from the proposed melt compositions of samples 40321 of EK-4 and 40271 of EK-2. The remaining units EK-5, EK-6, WK-3 and WK-4 define the second group of highly evolved KSC units (Figs. 4–6). These units define a decreasing trend in Fig. 4O from SiO_2 = 68 wt%. In contrast to the second group, WK-1 and WK-5 never have Eu/Eu* below 0.6 and Sr/Nd below 0.8 (Fig. 8A). Based on the hypothetical evolution curve for magmas more primitive than Kærven rocks in this diagram, some WK-1 and WK-5 rocks can be perceived as displaying near melt compositions, e.g. 66589 and 40303. Others are cumulates with notable losses of intercumulus liquid and have higher Eu/Eu*. This impression is reinforced in Fig. 11E, where these rocks also trend from possible near-melt compositions of e.g. 66589 and 40303 towards more accumulative types with higher Ba and lower Rb. The two magmas intruded to form units WK-1 and WK-5 are thus both indicated to have been somewhat more evolved than the WK-2 magma.

Among the high-silica units, WK-3 has very high concentrations of incompatible Rb, Zr, Th, and LREEs, and therefore a high content of interstitial melt. High Th/Rb and very low Ba, Sr, and Eu/Eu*, as well as K/Rb < 400 in three of the four samples in WK-3, indicate fractionation of alkali feldspar, and we interpret the overall composition of these rather similar rocks to be approximately the composition of the WK-3 magma.

EK-5 and EK-6 show an approximately equal and relatively large range of Rb, Th, Nb, Zr, and LREE (Fig. 5). However, in other respects EK-5 rocks seem consistently to have the hallmarks of an evolved end-member, with Ba < 200 ppm, Sr < 10 ppm, Sc < 3 ppm and Eu/Eu* < 0.2; SiO_2 is high (73–74 wt%), and all the other major elements except K_2O are very low, or at least represent the lowest values for KSC. The variable Rb, Th, Nb, Zr, and LREEs in EK-5 are clear indications of either variable fractions of a trapped liquid component in the rocks or crystallisation of accessory minerals. As the most silica-rich EK-5 and EK-6 rocks have the lowest K/Rb (< 400) they seem to be closest to thermal minimum melt compositions among KSC rocks. EK-6 rocks may be explained by mixing of an extremely enriched EK-5 melt and a liquidus mineral assemblage less evolved than that indicated for EK-5. WK-4 shows a significant interval of silica ranging as high as EK-5. Higher P_2O_5, MgO and Mg# at a given SiO_2 set WK-4 apart from EK-6, but it is also characteristic that towards the highest silica, WK-4 rocks tend to attain lower Th, Zr, Nb, and LREEs than EK-5. A high proportion of cumulus minerals and loss of interstitial melt is indicated for WK-4 by K/Rb > 400,

relatively low Ba, coupled with low Rb (Fig. 11) and, in some rocks, low Th/Rb. It therefore appears that the three most silica-rich units in the KSC were formed by individually different series of processes.

It is significant that some HFSE ratios show very limited variation for several granitic intrusive units. Zr/Hf is within 40–46 for EK-5, EK-6, WK-3, WK-4, and WK-5 (apart from one rock) and indicates that the accessory phase titanite did not fractionate or accumulate much during the formation of these rocks (Supplementary data file 2), as would otherwise be expected from average $K_d(Zr/Hf)^{titanite/melt} = 0.58$ and the high compatibility of these elements (Bachmann *et al.* 2005; Colombini *et al.* 2011; Padilla *et al.* 2016). This contrasts with the variability for WK-2 (Zr/Hf = 35–50) and EK-3 (Zr/Hf = 17–39). In addition, zircon fractionation lowered Zr/Nb as much as down to 1 (Supplementary data file 2) because of relatively low $K_d(Nb)^{zircon/melt} = 9$ (Padilla *et al.* 2016), but did not change Zr/Hf much because $K_d(Zr/Hf)^{zircon/melt}$ is near 1 (e.g. Rubatto & Hermann (2007) report an average of 1.08). We also note that most rocks of the mentioned granitic units show a remarkably tight cluster of Zr/Nb = 7–8.5, suggesting this to reflect melt compositions. The rise in Rb/Sr and strongly correlated decrease of Ba/Rb, Ba, and Sr of the rocks of the evolved units (Fig. 8C, D) with increasing SiO_2 (Fig. 5) is evidence for the role of alkali feldspar fractionation. The limited range of Ba/Sr = 10–15 in all the granitic units is probably an effect of a constant alkali feldspar/melt partitioning coefficient for these elements.

Two parental magmas for the late alkaline dykes

Compared to Group 1 dykes, Group 2 dykes are slightly more evolved with respect to Fe/Mg and are richer in FeO^{total} and MnO. Some trace elements are relatively enriched in Group 2 dykes: Nb, Zr, Pb, Th, U, Cs and La. Group 2 dykes also have higher $La/Sm_{cho} \approx 9$ (Group 1 has ≈ 5), La/Nb = 0.66–0.87 (Group 1: 0.89–0.96), Nb/Ta ≈ 23 (Group 1: 15) and Zr/Hf = 48 (Group 1: 43), whereas Group 1 has much more fractionated HREEs with $Tb/Yb_{cho} = 3.1–3.4$ (Group 2: ≈ 2.1). The latter is coupled to relatively higher Pr-Dy in Group 1 rocks. Group 2 has $Eu/Eu^* \approx 0.90$, whereas Group 1 has 0.59–0.61, possibly reflecting that plagioclase did not fractionate in the most silica undersaturated parental melts. These fine-grained rocks with limited phenocryst content probably approximate melt compositions. Irrespective of the presumed long path of magmatic differentiation, the consistent differences between the two groups of late dykes suggest they were derived from separate magmatic compositions, presumably linked to mantle sources at different depths and of different degree and style of enrichments.

A model for magmatic plumbing and emplacement beneath Kærven

Bearing in mind the suggested cumulative nature of a number of Kærven syenite samples, which consequently do not represent actual melt compositions, the overall temporal geochemical evolution at Kærven is illustrated in Fig. 12. The figure shows sample ranges and SiO_2 for inferred near-melt compositions for individual units plotted against the relative sequence of intrusion for the eastern and western Kærven intrusive units.

The range of bulk rock compositions, and the reversals to less evolved compositions with time at both East and West Kærven, require the existence of more than one magma at depth. For West Kærven we note two geochemical reversals signalling introduction of less evolved magma into the system: one following the intrusion of the WK-1 granite and one leading to the intrusion of the youngest West Kærven unit, the WK-5 granite. In East Kærven, a shift to less evolved compositions is marked before the emplacement of the youngest East Kærven unit, the EK-6 granites.

Geochemical correlation between East and West Kærven is, as shown by Harker diagrams, not obvious. It is, however, clear that the youngest mapped unit in each sector requires emplacement of less evolved compositions from the feeder systems. The resulting compositions (WK-5 granite and EK-6 granite) are, however, far from identical. It therefore emerges that the final geochemical reversals at East and West Kærven are either not contemporary, or that the East and West Kærven successions originate from different magma chambers.

East Kærven. Although the intimate association of EK-1 with the basement could point to EK-1 as representing the earliest East Kærven intrusive unit, the lack of internal contacts in the quartz syenites lead us to consider the EK-1 and EK-2 as coeval units one of which has interacted with the Precambrian host rocks. The subsequently emplaced EK-3 and EK-4 syenites have geochemical characteristics which do not exclude an origin from magma similar to that responsible for earlier EK-1 and EK-2 quartz syenites. The less cumulative EK-4 rocks occur centrally in the ring dyke of EK-3 (see position of EK-4 samples (Supplementary data file 1) on the map in Supplementary data file 2), and this suggests that the EK-4 magma, which was less evolved than the magma from which EK-3 cumulates formed, was intruded as a late pulse of magma into the EK-3 mush. During this process, the intercumulus melt of EK-3 was replaced by the

incoming magma in extents decreasing laterally away from the intrusive center. The following EK-5 granite, among the most evolved compositions at Kærven, could conceivably be generated by extensive fractionation of melts from the EK-3/EK-4 magmatic system. A return to less evolved compositions in the last emplaced East Kærven unit, EK-6, requires replenishment of the magma chamber from which the East Kærven units were derived.

West Kærven. Deriving the WK-2 syenites from the oldest WK-1 granitic magma at West Kærven requires inflow of more primitive magma into the deep chamber where the WK-1 magma resided before intrusion at KSC level. Alternatively, WK-1 represents a localised evolved facies of the West Kærven magma chamber from which the less evolved WK-2 unit was subsequently derived. In this scenario, tapping of a second evolved portion of the West Kærven magma chamber is needed for the derivation of unit WK-3. The subsequently emplaced WK-4 granites are more evolved than both WK-1 and WK-3. As it seems unlikely that WK-4 could be generated by introducing alkali feldspar cumulus crystals into a WK-3 melt, a third evolved and distinct portion of the magma chamber is needed to generate the WK-4 compositions. The final WK-5 granites mark a return to emplacement of less evolved melts. As these are not identical to the earlier WK-1 granites, replenishment of the magma chamber with less evolved magma is required in order to generate the WK-5 magmas. Alternatively, the WK-5 rocks could be derived from a different magma chamber than the previous West Kærven intrusives.

In summary, we propose that the felsic units at Kærven were derived from a number of geochemically different magmas evolving in up to three separate chambers, with one chamber linked to the East Kærven and one or two chambers to the West Kærven successions. Moreover, it seems likely that the East and West Kærven syenites and granites evolved independently. The late and geochemically distinct, highly alkaline green dykes represent a development at KSC that is not related to the rest of the KSC but is more similar to the KAI. The dykes represent two different, highly silica-undersaturated magmas which, however, are unlike the main rocks of the KAI and therefore not necessarily directly related to the evolution of the KAI.

Origin of parental magmas

Nielsen (1987) presented a comprehensive set of models for the Tetiary formation of alkaline magmas in East Greenland. The ultimate source was plume asthenosphere which melted to a limited extent due to thick lithosphere outside the continental rifted margin, where tholeiitic magma formed. In the modelling of Nielsen (1987, Fig. 14) the KSC would be an example of "Lineage XII" derived from trachybasaltic magma evolving in the crust.

The best approximations to melt compositions for the KSC units with the least evolved rocks are trachytic, EK-2 sample 40271 with 64.1 wt% SiO_2, WK-2 sample 66525 with 63.6 wt% SiO_2, and EK-4 sample 40321 with 66.4 wt% SiO_2 (Table 2, Fig. 4). WK-5 sample 66589 with 66.7 wt% SiO_2 and WK-3 sample 66614

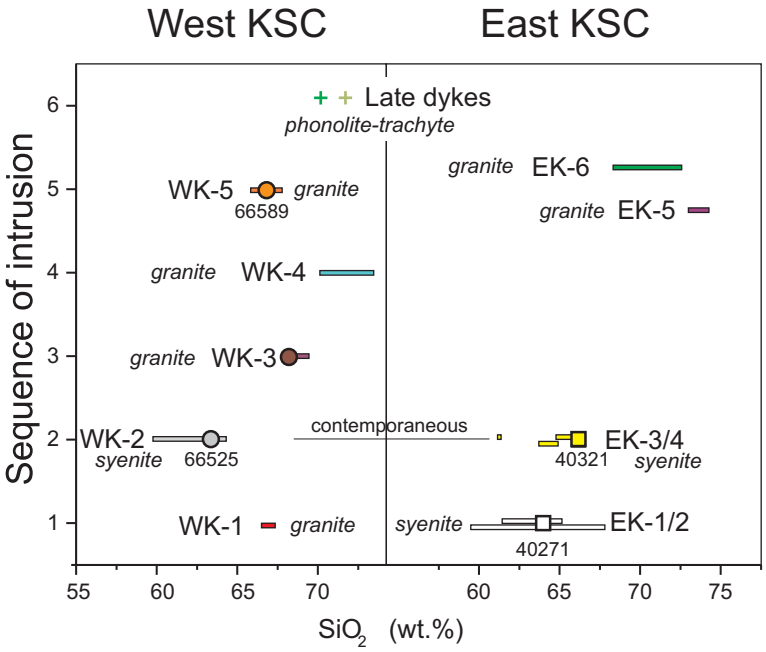

Fig. 12. Sequence of intrusion of the KSC units with SiO_2 compositional ranges and indicated approximate liquid compositions (coloured symbols). Numbering on the y-axis refers to the western units. EK-6 is later than WK-5.

with 67.9 wt% SiO_2 have also been argued to resemble melts and are only slightly more evolved.

All of these rocks are much more evolved than any magma directly derived from the mantle. Moreover, all are partial cumulates (e.g. with K/Rb > mantle rocks, Fig. 11A), and in our modelling each of them has lost a certain fraction of late interstitial melt. However, we argue that the sum of the cumulus minerals and the final trapped melt in these rocks has a composition not very different from the intruded magma. This is illustrated by the fact that their compositions lie close to the modelled melt evolution curves in Fig. 11.

Considering the geological setting of the KSC near the Palaeogene continental rifted margin and possibly more or less positioned in the failed arm of a triple junction (Fig. 1; Brooks 1973), we discuss below three possible scenarios for the origin of the parental melts to the KSC.

Partial melts from Archaean crustal lithologies

Presumed anatectic partial melts of the basement gneisses suggested to be formed during emplacement of the Miki Fjord macrodike complex have been described by Blichert-Toft *et al.* (1992). These frozen granophyric melts sit between the hybridised basement and the macrodike. They have granitic compositions with low alkalis and high MgO as well as high Ba, Sr, and Rb but low Zr and Y compared to KSC granites. They are therefore geochemically quite unlike the potential parental compositions to the KSC outlined above. A large fraction of basic material added to the anatectic melt would be needed to obtain major element compositions approaching the KSC parents. Neither the abundances of the above-mentioned trace elements, nor the high mantle-like oceanic ratios of Nb/U and Ce/Pb in the KSC melts can be produced by mixing basement or basement melts with basaltic melts known from the North Atlantic Igneous Province. We therefore consider such a hybrid origin very unlikely.

Extensive fractionation of basaltic melts derived from the Tertiary Icelandic mantle plume

Very few reported magmatic compositions from the East Greenland Palaeogene come close to the suggested Kærven magma compositions. Scoresby Sund flood basalts have invariably <55 wt% SiO_2 (Larsen *et al.* 1989), as do the majority of the Lower Lavas. However, a few Lower Lavas from the Vandfaldsdalen Formation and a flow from the Milne Land Formation in the southern Prinsen af Wales Bjerge have SiO_2 in the range 55–58 wt% SiO_2 (Hansen & Nielsen 1999; Hansen *et al.* 2002). Along with a granophyre (58.9 wt% SiO_2) from the felsic series of the Vandfaldsdalen Macrodyke (White *et al.* 1989), these rocks indicate that relatively high-SiO_2 liquids were available in the province both during flood basalt volcanism and the subsequent geological evolution. However, all these somewhat evolved melts have relatively low Al_2O_3 contents (12.2–13.9 wt%), which would be expected to become even lower at the silica levels of the KSC magmas and thus far below the 13.4–15.5 wt% Al_2O_3 of KSC magmas.

Relatively high Al_2O_3 is present in the Transitional Series (TRANS) dykes of Hanghøj *et al.* (2003), which were intruded later than the flood basalts. However, the TRANS dykes all have MgO > 3 wt% and SiO_2 < 54 wt%, and any correlation with KSC magmas cannot be ascertained. The diorite plugs of ABC (Riishuus *et al.* 2005) resemble the TRANS of Hanghøj *et al.* (2003) in several respects, including relatively high Al_2O_3. Although suggested to be the least contaminated of the ABC rocks, the diorites were still considered to be severely crustally contaminated by Riishuus *et al.* (2005). Differentiated and oversaturated members of the late dyke swarm (Brooks & Platt 1975) emplaced after the KAI have appropriate SiO_2 and Al_2O_3 contents, but we have no information suggesting that such compositions were available in the area in pre-KAI times. The ALK-1 dykes in the outer part of the Kangerlussuaq area (Nielsen 1978) are marginally alkaline but have relatively low Al_2O_3 and distinguish themselves from the TRANS of Hanghøj *et al.* (2003) by their higher TiO_2 at comparable Mg#. One TRANS-1 dyke of Nielsen (1978) has silica in the range of KSC magmas but has lower alkalis.

To further characterise the parental KSC melts we compare three selected trace element ratios of the KSC magmas with other igneous rocks of presumed approximate melt compositions in the Kangerlussuaq area, as well as other occurrences related to the Iceland mantle plume or Greenland continental rifting in the Palaeogene (Fig. 13). Even for very evolved melts La/Nb probably closely approximates to the ratio of the melt source. La/Nd and Zr/Nb, on the other hand, may be considerably fractionated during a low degree of partial mantle melting, but the estimated change during magmatic differentiation from basalt to the KSC magma compositions discussed is limited to not more than around 10–15 %, assuming clinopyroxene is the only significant phase fractionating these ratios, and assuming around 30 % clinopyroxene in the total crystallising assemblage. We use the ratios to compare characteristics of the parental melts. East Greenland flood basalts and Icelandic rocks of both tholeiitic and alkaline type less evolved than the KSC melts typically have higher Zr/Nb than the KSC melts, and the samples with low Zr/Nb also have lower La/Nb than the KSC (Fig. 13A). Among Palaeogene tholeiitic lavas

and dykes from this region of East Greenland few are comparable to KSC rocks in Fig. 13; the tholeiitic rocks of macrodykes of the Kangerlussuaq area of type Thol-2 (Nielsen 1978) resemble the East Greenland flood basalts, as also discussed by Holm *et al.* (2006). These trace element ratios also set KSC apart from the Kærven Gabbro, as indicated by samples from a presumed feeder channel for the gabbro, a related macrodyke, and a late gabbroic pegmatite in the gabbro (Fig. 13B). It therefore seems that the KSC magmas are unrelated to the magmas of the Kærven gabbro, as well as to other local mafic rocks related to the flood basalt magmatism of the East Greenland continental margin during breakup.

The geochemical deviation of the Kærven rocks from those of Iceland is also manifested by consideration of the respective Fe-enrichment trends (Fig. 4C, O). Charreteur *et al.* (2013) have suggested that the intermediate and silicic rocks from Thingmuli and other Icelandic volcanoes evolved along two trends identified by low and high Fe-enrichment, respectively, and that a compositional gap exists between these compositions. The Kærven inferred approximate melt compositions depart from this scheme and plot generally within the compositional gap in the Iceland data (Fig. 4J).

Extensive fractionation of basaltic melts derived from an enriched source in the lithospheric mantle, possibly with a component of plume melt

Several lines of evidence indicate that the Kærven rocks are unlikely to be closely associated with

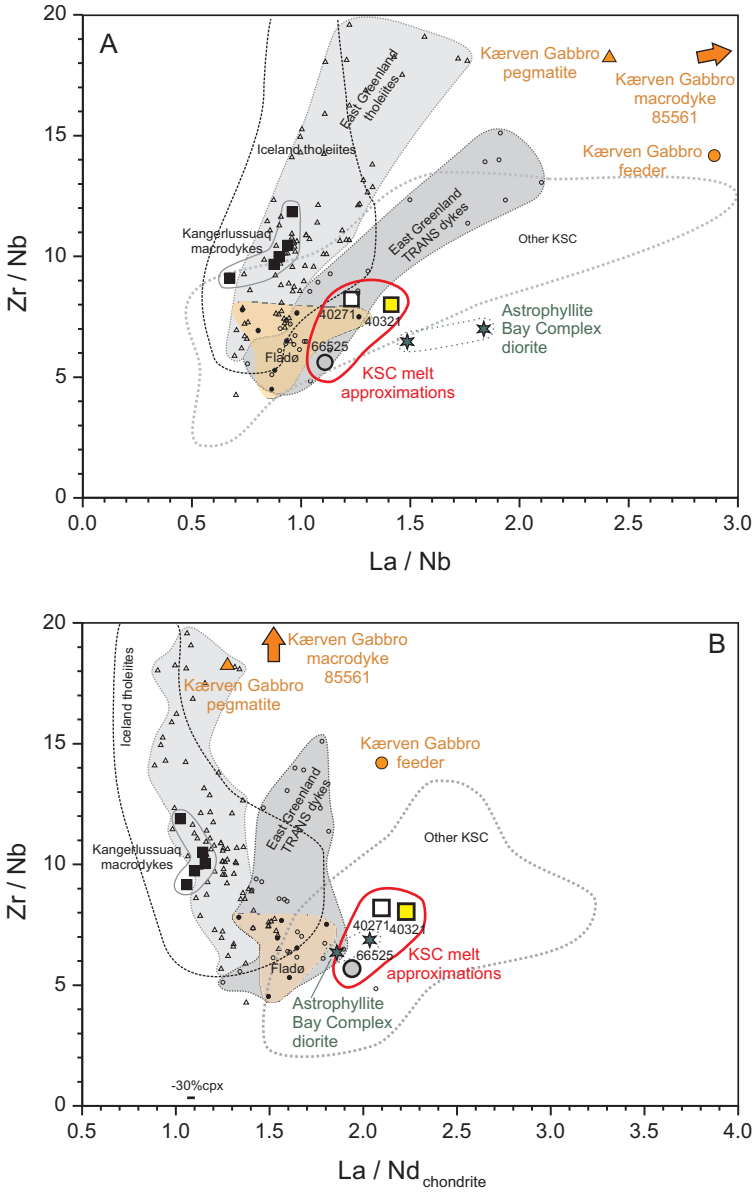

Fig. 13. Comparison of suggested KSC melts with selected other inferred magma compositions from the Kærven area, the Kangerlussuaq fjord area, the East Greenland Tertiary Igneous Province and Iceland. **A**: Zr/Nb vs. La/Nb; **B**: Zr/Nb vs. $La/Nd_{chondrite}$; in B, the point labelled –30% cpx is the effect of fractionation of 30 % clinopyroxene. Data for Kangerlussuaq macrodykes and the Kærven gabbro feeder, pegmatite and macrodyke are from Holm *et al.* (2006). Diorites from the Astrophyllite Bay Complex are from Riishuus *et al.* (2005); East Greenland TRANS dykes including Fladø dykes are from Hanghøj *et al.* (2003), and the fields for Iceland and East Greenland tholeiites are from GEOROC (2018). Other KSC is from the present work. See text for discussion.

known Icelandic magma compositions or compositions related to the Palaeogene flood basalt volcanism of the East Greenland margin. The KSC melts must have an origin in materials with Nb/U and Ce/Pb as in oceanic basalts and their sources. Their tholeiitic character may suggest that they were not derived by a significantly lower degree of melting than basaltic rocks of the Kangerlussuaq area. The lower Zr/Nb would then point to a more incompatible-element enriched source, but not one with the character of a typical OIB source with La/Nb < 1 (e.g. Willbold & Stracke 2006). The high La/Nd_{cho} = 1.9–2.2 in KSC melts compared to 1.0–1.3 in e.g. Kangerlussuaq basaltic dykes also points to a more enriched source. Thus KSC melts have compositions that deviate somewhat from many plume type magmas. Significantly, the HREEs are moderately fractionated, indicating that the major part of the melts were generated more shallowly than in a garnet-bearing source. Values of Tb/Yb_{cho} = 1.8–2.0 for KSC melt approximations are as found in Icelandic flank zone magmas and magmas of the propagating south-east rift (e.g. Peate *et al.* 2010) and in some East Greenland plateau lavas (e.g. Fram & Lesher 1993; Tegner *et al.* 1998; Peate *et al.* 2003). Thus, in accord with other presented evidence, melting in the lithospheric mantle is indicated unless lithospheric thinning had taken place of the presumably thick pre-rift Archaean lithosphere to an extent allowing asthenosphere to melt. The rather dry character (Holm & Prægel 1988a), and relatively low K_2O/Na_2O of 0.9–1.0 of the melts do not indicate amphibole-rich metasomatic veins as mantle source rocks (e.g. Pilet *et al.* 2008) and even less a biotite-rich source. Instead, we speculate that the sources were veins precipitated from comparatively dry metasomatising basaltic magmas, and that these were mobilised due to the heating from the Iceland plume at the bottom of the lithosphere or by the passing of plume-derived magmas.

The TRANS dykes (Hanghøj *et al.* 2003), which include dykes at Fladø at the mouth of Kangerlussuaq, formed late in the development of the coast-parallel dyke swarm, and these may be coeval with KSC and include basaltic parental melts for KSC. They are relatively enriched in incompatible trace elements (Hanghøj *et al.* 2003), are marginally silica saturated, plot near the inferred KSC magmas in Fig. 13, and have higher Al_2O_3 at low MgO than the flood basalts, which have too low alumina to qualify as parental to KSC magmas. Due to lack of trace element data, the ALK-1 dykes of the Kangerlussuaq area cannot be characterised but may prove to be a local development of the regional TRANS dykes. Hanghøj *et al.* (2003) evaluated a lithospheric mantle origin for TRANS dykes, but favoured crustal contamination to explain the variation of radiogenic isotopes and La/Nb ratios in these post-breakup tholeiitic magmas. We note that the TRANS dykes have high Ce/Pb and Nb/U ratios, typical of oceanic magmas, which would only allow a few percent contamination by the continental crust in their model. This contrasts to the required 10–20 % crust derived from consideration of La/Nb and Nd isotopic compositions in the modelling of Hanghøj *et al.* (2003). We therefore suggest that both the KSC magmas and the TRANS dyke magmas may be part of the same mantle melting events near the base of thinned Archaean lithospheric mantle at the latest stage of continental breakup.

We also note that the diorite plugs at ABC (Riishuus *et al.* 2005) have La/Nd and Zr/Nb resembling the approximate KSC melts, and slightly higher La/Nb (Fig. 13). These diorites were proposed to be severely contaminated by granulite (Riishuus *et al.* 2005), but they have Nb/U > 100 and Ce/Pb around 20 which cannot be reconciled with strong contamination with continental crust. Instead, the trace elements suggest that the ABC diorites formed from magmas not much different from KSC magmas.

Conclusions

The Kærven Syenite Complex (KSC) consists primarily of 11 felsic intrusions emplaced in the form of ring dykes in the Archaean basement subsequent to intrusion of the Kærven Gabbro and before the emplacement of the Kangerlussuaq Alkaline Intrusion (KAI). The KSC magmas evolved by crystal fractionation in crustal magma chambers at depth prior to emplacement.

KSC is the only felsic complex in the Kangerlussuaq area with an extensive compositional range from quartz syenite through syenite and alkali feldspar syenite to alkali feldspar granite.

Combined field and geochemical data show that at least three separate magmas, possibly evolving in different chambers, are required to explain the formation of the KSC.

Individual intrusive units of KSC display limited compositional variation, and the variation within several of the intrusive units can be explained by *in situ* crystallisation, partial crystallisation of interstitial melt, followed by partial loss of highly evolved residual interstitial melt.

Modelling of the WK-2 unit suggests that in a crystal–liquid mush initially a dioritic mineral paragenesis formed and was followed by an alkali feldspar syenitic, which left around 40 % melt in the mush. Variable fractions of this melt were lost to develop the variable characteristics of the WK-2 syenites.

The formation of units EK-3 and EK-4 rocks requires replacement of the original, very evolved, interstitial liquid with less evolved liquid.

The magma of the early EK-1 quartz syenites underwent extensive crustal contamination due to partial assimilation of local basement gneiss; this process was limited to the earliest stage of intrusion at KSC.

KSC magmas were derived from incompatible-element enriched parental compositions which were dissimilar to other reported local, regional or Icelandic basaltic magmas except for TRANS dykes (*sensu* Hanghøj *et al*. 2003) and possibly the diorites of the Astrophyllite Bay Complex (Riishuus *et al*. 2005). KSC magmas are suggested to be of lithospheric mantle origin.

Late dykes in KSC are peralkaline phonolitic and trachytic and can be divided into two groups, both of which have affinity to KAI foyaites but are geochemically distinct from any known KAI unit. They seem distinct from green dykes common throughout the Kangerlussuaq region.

Acknowledgements

We thank GEUS for major element analyses and the topographic map of the Kærven area. John Bailey (Department of Geosciences and Natural Resource Management, University of Copenhagen) kindly supplied the trace element data by XRF. We are grateful for the thorough reviews and constructive suggestions of Troels Nielsen and Richard Wilson, as well as for the review and thorough editorial handling by Lotte Melchior Larsen – they all improved the manuscript significantly. Our work in East Greenland has been supported by grants from the Independent Research Fund Denmark and the Carlsberg Foundation.

References

Bachmann, O. & Huber, C. 2016: Silicic magma reservoirs in the Earth's crust. American Mineralogist 101, 2377–2404.

Bachmann, O., Dungan, M.A. & Bussy, F. 2005: Insights into shallow magmatic processes in large silicic magma bodies: The trace element record in the Fish Canyon magma body, Colorado. Contributions to Mineralogy and Petrology 149, 338–349. doi: 10.1007/s00410-005-0653-z

Barberi, F., Ferrara, G., Santacroce, R., Treuil, M. & Varet, J. 1975: A Transitional Basalt-Pantellerite Sequence of Fractional Crystallization, the Boina Centre (Afar Rift, Ethiopia). Journal of Petrology 16, 22–56.

Becker, A., Holtz, F. & Johannes, W. 1998: Liquidus temperatures and phase compositions in the system Qz-Ab-Or at 5 kbar and very low water activities. Contributions to Mineralogy and Petrology 130, 213–224. doi: 10.1007/s004100050361

Bird, D.K., Rosing, M.T., Manning, C.E. & Rose, N.M. 1985: Geologic field studies of the Miki Fjord Area, East Greenland. Bulletin of the Geological Society of Denmark 34, 219–236.

Blichert-Toft, J., Lesher, C.E. & Rosing, M.T. 1992: Selectively contaminated magmas of the Tertiary East Greenland macrodike complex. Contributions to Mineralogy and Petrology 110, 154–172.

Bridgwater, D., Davies, F.B., Gill, R.C.O., Gorman, B.E., Myers, J.S., Pedersen, S. & Taylor, P.N. 1978: Field work between Kangerdlugssuaq and Angmagssalik Ø, South-East and southern East Greenland. Rapport Grønlands Geologiske Undersøgelse 90, 87–89.

Brooks, C.K. 1973: Rifting and Doming in Southern East Greenland. Nature Physical Science 244, 23–25.

Brooks, C.K. 1991: The Kræmer Ø syenite, Kangerdlugssuaq: preliminary description of one of the voluminous oversaturated syenites of the East Greenland Tertiary. Bulletin of the Geological Society of Denmark 38, 145–151.

Brooks, C.K. 2011: The East Greenland rifted volcanic margin. Geological Survey of Denmark and Greenland Bulletin 24, 1–96.

Brooks, C.K. & Nielsen, T.F.D. 1982: The Phanerozoic development of the Kangerdlugssuaq area, East Greenland. Meddelelser om Grønland, Geoscience 9, 32 pp.

Brooks, C.K. & Platt, R. 1975: Kaersutite-bearing gabbroic inclusions and the late dike swarm of Kangerdlugssuaq, East Greenland. Mineralogical Magazine 40, 259–283.

Brooks, C.K. & Rucklidge, J.C. 1974: Strongly undersaturated Tertiary volcanic rocks from the Kangerdlugssuaq area, east Greenland. Lithos 7, 239–248. DOI: 10.1016/0024-4937(74)90045-0

Brooks, C.K. & Rucklidge, J.C. 1976: Tertiary peralkaline rhyolite dikes from the Skærgaard area, Kangerdlugssuaq, East Greenland. Meddelser om Grønland 197(3), 1–27.

Carmichael, I.S.E. 1964: The Petrology of Thingmuli, a Tertiary Volcano in Eastern Iceland. Journal of Petrology 5, 435–460.

Charreteur, G., Tegner, C. & Haase, K. 2013: Multiple ways of producing intermediate and silicic rocks within Thingmúli and other Icelandic volcanoes. Contributions to Mineralogy and Petrology 166, 471–490. doi: 10.1007/s00410-013-0886-1

Colombini, L.L., Miller, C.F., Gualda, G.A.R., Wooden, J.L. & Miller, J.S. 2011: Sphene and zircon in the Highland Range volcanic sequence (Miocene, southern Nevada, USA): Elemental partitioning, phase relations, and influence on evolution of silicic magma. Mineralogy and Petrology 102, 29–50. doi: 10.1007/s00710-011-0177-3

Deer, W.A. 1976: Tertiary igneous rocks between Scoresby Sund and Kap Gustav Holm, East Greenland. In: Escher, A. & Watt, W.S. (eds), Geology of Greenland, 406–429. Copenhagen: Grønlands Geologiske Undersøgelse.

Deer, W.A. & Kempe, D.R.C. 1976: Geological investigations in East Greenland: Part XI: The minor peripheral intrusions,

Kangerdlugssuaq, East Greenland. Meddelelser om Grønland 197(4), 1–25.

Deer, W.A., Kempe, D.R.C. & Jones, G.C. 1984: Syenitic and associated intrusions of the Kap Edvard Holm region of Kangerdlugssuaq, East Greenland. Meddelelser om Grønland, Geoscience 12, 1–26.

Deering, C.D. & Bachmann, O. 2010: Trace element indicators of crystal accumulation in silicic igneous rocks. Earth and Planetary Science Letters 297, 324–331. doi: 10.1016/j.epsl.2010.06.034

Flude, S., Burgess, R. & McGarvie, D.W. 2008: Silicic volcanism at Ljósufjöll, Iceland: Insights into evolution and eruptive history from Ar-Ar dating. Journal of Volcanology and Geothermal Research 169, 154–175.

Fram, M.S. & Lesher, C.E. 1993: Geochemical constraints on mantle melting during creation of the North Atlantic basin. Nature 363, 712–715.

Frost, B.R., Barnes, C.G., Collins, W.J., Arculus, R.J., Ellis, D.J. & Frost, C.D. 2001: A Geochemical Classification for Granitic Rocks. Journal of Petrology 42, 2033–2048.

GEOROC 2018: Available at: http://georoc.mpch-mainz.gwdg.de/georoc/. Last accessed 17.08.2018.

Ghiorso, M.S. & Sack, R.O. 1995: Chemical mass transfer in magmatic processes IV. A revised and internally consistent thermodynamic model for the interpolation and extrapolation of liquid-solid. Contributions to Mineralogy and Petrology 119, 197–212. doi: 10.1007/BF00307281

Gwozdz, R., Hansen, H.J., Rasmussen, K.L. & Kunzendorf, K. 1993: Instrumental neutron activation analysis of samples with masses from micrograms to hectograms. Journal of Radioanalytical and Nuclear Chemistry 167, 161–168.

Hanghøj, K., Storey, M. & Stecher, O. 2003: An Isotope and Trace Element Study of the East Greenland Tertiary Dyke Swarm: Constraints on Temporal and Spatial Evolution during Continental Rifting. Journal of Petrology 44, 2081–2112.

Hansen, H. & Nielsen, T.F.D. 1999: Crustal contamination in Palaeogene East Greenland flood basalts: Plumbing system evolution during continental rifting. Chemical Geology 157, 89–118. doi: 10.1016/S0009-2541(98)00196-X

Hansen, H., Pedersen, A.K., Duncan, R.A., Bird, D.K., Brooks, C.K., Fawcett, J.J., Gittins, J., Gorton, M. & O'Day, P. 2002: Volcanic stratigraphy of the southern Prinsen af Wales Bjerge region, East Greenland. In: Jolley, D.W. & Bell, B.R. (eds), The North Atlantic Igneous Province: Stratigraphy, Tectonic, Volcanic and Magmatic Processes. Geological Society Special Publications 197, 183–218. doi: 10.1144/GSL.SP.2002.197.01.08

Hofmann, A.W. 2003: Sampling Mantle Heterogeneity through Oceanic Basalts: Isotopes and Trace Elements. In: Holland, H. & Turekian, K. (eds), Treatise on Geochemistry vol. 2, 61–101. Oxford: Elsevier-Pergamon.

Holm, P.M. 1990: Radiometric age determinations in the Kærven area, Kangerdlugssuaq, East Greenland Tertiary igneous province; $^{40}Ar/^{39}Ar$, K/Ar and Rb/Sr isotopic results. Bulletin of the Geological Society of Denmark 38, 183–201.

Holm, P.M. & Prægel, N.-O. 1988a: The Tertiary Kærven syenite complex, Kangerdlugssuaq, East Greenland: mineral chemistry and geochemistry. Mineralogical Magazine 52, 435–450.

Holm, P.M. & Prægel, N.-O. 1988b: Rare earth element geochemistry of the Kærven syenite complex, Kangerdlugssuaq, East Greenland. In: Binzer, K., Marcussen, I. & Konradi, P. (eds), Abstracts 18. Nordiske Geologiske Vintermøde, 171–172.

Holm, P.M., Prægel, N.-O., Hansen, E.R., Dahlstrøm, K. & Pedersen, M. 1990: Results of geological investigations of the Tertiary Intrusions in the Kærven area. In: Brooks, C.K. (ed), Kangerdlugssuaq Studies: Processes at a Rifted Continental Margin, 56–61. København: Geologisk Centralinstitut.

Holm, P.M., Prægel, N.-O. & Egeberg, E.D. 1991: Multiple syenite intrusions at Kærven, Kangerdlugssuaq, East Greenland: Evidence from the 1986 field work. Bulletin of the Geological Society of Denmark 38, 173–181.

Holm, P.M., Heaman, L.M. & Pedersen, L.E. 2006: Baddeleyite and zircon U-Pb ages from the Kærven area, Kangerlussuaq: Implications for the timing of Paleogene continental breakup in the North Atlantic. Lithos 92, 238–250.

Icenhower, J. & London, D. 1996: Experimental partitioning of Rb, Cs, Sr, and Ba between alkali feldspar and peraluminous melt. American Mineralogist 81, 719–734.

Iezzi, G., Mollo, S., Ventura, G., Cavallo, A. & Romano, C. 2008: Experimental solidification of anhydrous latitic and trachytic melts at different cooling rates: The role of nucleation kinetics. Chemical Geology 253, 91–101. doi: 10.1016/j.chemgeo.2008.04.008

Jackson, E.D. 1961: Primary Textures and Mineral Associations in the Ultramafic Zone of the Stillwater Complex, Montana. Geological Survey Professional Paper 358, 103 pp.

James, R.S. & Hamilton, D.L. 1969: Phase relations in the system $NaAlSi_3O_8$-$KAlSi_3O_8$-$CaAl_2Si_2O_8$-SiO_2 at 1 kilobar water vapour pressure. Contributions to Mineralogy and Petrology 21, 111–141. doi: 10.1007/BF00403341

Jochum, K.P. & Nehring, F. 2006: GeoReM preferred Values. 11/2006. http://georem.mpch-mainz.gwdg.de

Jónasson, K. 2007: Silicic volcanism in Iceland: Composition and distribution within the active volcanic zones. Journal of Geodynamics 43, 101–117. doi: 10.1016/j.jog.2006.09.004

Kystol, J. & Larsen, L.M. 1999: Analytical procedures in the Rock Geochemical Laboratory of the Geological Survey of Denmark and Greenland. Geology of Greenland Survey Bulletin 184, 59–62.

Langmuir, C.H. 1989: Geochemical consequences of in situ crystallization. Nature 340, 199–205.

Larsen, L.M., Watt, W.S. & Watt, M. 1989: Geology and petrology of the Lower Tertiary plateau basalts of the Scoresby Sund region, East Greenland. Bulletin Grønlands Geologiske Undersøgelse 157, 164 pp.

Le Maitre, R.W. 1989: A classification of igneous rocks and glossary of terms. Oxford: Blackwell Scientific Publications.

Lee, C.T.A. & Morton, D.M. 2015: High silica granites: Terminal porosity and crystal settling in shallow magma chambers. Earth and Planetary Science Letters 409, 23–31. doi: 10.1016/j.epsl.2014.10.040

Lundstrom, C.C. & Glazner, A.F. 2016: Silicic Magmatism and the Volcanic–Plutonic Connection. Elements 12, 91–96.

Luth, W.C. 1969: The Systems $NaAlSi_3O_8$–SiO_2 and $KAlSi_3O_8$–SiO_2 to 20 kb and the Relationship between H_2O Content, PH_2O and Ptotal in Granitic Magmas. American Journal of Science 267A, 325–341.

Mahood, G.A. 1981: Chemical evolution of a pleistocene rhyolitic center: Sierra La Primavera, Jalisco, México. Contributions to Mineralogy and Petrology 77, 129–149.

Martin, E. & Sigmarsson, O. 2007: Crustal thermal state and origin of silicic magma in Iceland: the case of Torfajökull, Ljósufjöll and Snæfellsjökull volcanoes. Contributions to Mineralogy and Petrology 153, 593–605.

McBirney, A.R. & Noyes, R.M. 1979: Crystallization and Layering of the Skaergaard Intrusion. Journal of Petrology 20, 487–554.

Naney, M.T. & Swanson, S.E. 1980: The effect of Fe and Mg on crystallization in granitic systems. American Mineralogist 65, 639–653.

Nielsen, T.F.D. 1978: The Tertiary Dike Swarms of the Kangerdlugssuaq Area, East Greenland. Contributions to Mineralogy and Petrology 67, 63–78.

Nielsen, T.F.D. 1987: Tertiary alkaline magmatism in East Greenland: a review. In: Fitton, J.G. & Upton, B.G.J. (eds), Alkaline Igneous Rocks. Geological Society Special Publications 30, 489–515.

Ojha, D.N. 1966: Petrology of the Kærven Layered Intrusion, East Greenland. Journal of the Geochemical Society of India 1, 86–112.

Padilla, A.J. & Gualda, G.A.R. 2016: Crystal-melt elemental partitioning in silicic magmatic systems: An example from the Peach Spring Tuff high-silica rhyolite, Southwest USA. Chemical Geology 440, 326–344. doi: 10.1016/j.chemgeo.2016.07.004

Peate, D.W. Baker, J.A., Blichert-Toft, J., Hilton, D.R., Storey, M., Kent, A.J.R., Brooks, C.K., Hansen, H., Pedersen, A.K. & Duncan, R.A.. 2003: The Prinsen af Wales Bjerge Formation Lavas, East Greenland: the Transition from Tholeiitic to Alkalic Magmatism during Palaeogene Continental Break-up. Journal of Petrology 44, 279–304. doi: 10.1093/petrology/44.2.279

Peate, D.W., Breddam, K., Baker, J.A., Kurz, M.D., Barker, A.K., Prestvik, T., Grassineau, N. & Skovgaard, A.C. 2010: Compositional Characteristics and Spatial Distribution of Enriched Icelandic Mantle Components. Journal of Petrology 51, 1447–1475.

Petford, N., Cruden, A.R., McCaffrey, K.J.W. & Vigneresse, J.L. 2000: Granite magma formation, transport and emplacement in the Earth's crust. Nature 408, 669–673.

Philpotts, J.A. & Schnetzler, C.C. 1970: Phenocryst-matrix partition coefficients for K, Rb, Sr and Ba, with applications to anorthosite and basalt genesis. Geochimica et Cosmochimica Acta 34, 307–322. doi: 10.1016/0016-7037(70)90108-0

Piilonen, P.C., Lalonde, A.E., McDonald, A.M., Gault, R.A. & Larsen, A.O. 2003: Insights into astrophyllite-group minerals. I. Nomenclature, composition and development of a standardized general formula. Canadian Mineralogist 41, 1–26.

Pilet, S., Baker, M.B. & Stolper, E.M. 2008: Metasomatized Lithosphere and the Origin of Alkaline Lavas. Science 320, 916–919.

Prægel, N.-O. & Holm, P.M. 2001: Replenishment episodes and crustal assimilation in the development of an early Tertiary magma chamber, East Greenland: evidence from layered cumulates of the Kælvegletscher ultramafic complex, Kangerlussuaq. Mineralogy and Petrology 73, 279–304.

Riishuus, M.S., Peate, D.W., Tegner, C., Wilson, J.R., Brooks, C.K. & Waight, T.E. 2005: Petrogenesis of syenites at a rifted continental margin: origin, contamination and interaction of alkaline mafic and felsic magmas in the Astrophyllite Bay Complex, East Greenland. Contributions to Mineralogy and Petrology 149, 350–371.

Riishuus, M.S., Peate, D.W., Tegner, C., Wilson, J.R., Brooks, C.K. & Harris, C. 2006: Temporal evolution of a long-lived syenitic centre: The Kangerlussuaq Alkaline Complex, East Greenland. Lithos 92, 276–299.

Riishuus, M.S., Peate, D.W., Tegner, C., Wilson, J.R. & Brooks, C.K. 2008: Petrogenesis of cogenetic silica-oversaturated and -undersaturated Syenites by periodic recharge in a crustally contaminated magma chamber: the Kangerlussuaq intrusion, East Greenland. Journal of Petrology 49, 493–522.

Rose, N.M. & Bird, D.K. 1994: Hydrothermally altered dolerite dykes in East Greenland: implications for Ca-metasomatism of basaltic protoliths. Contributions to Mineralogy and Petrology 116, 420–432.

Rubatto, D. & Hermann, J. 2007: Experimental zircon/melt and zircon/garnet trace element partitioning and implications for the geochronology of crustal rocks. Chemical Geology 241, 38–61. doi: 10.1016/j.chemgeo.2007.01.027

Rudnick, R.L. & Gao, S. 2003: Composition of the Continental Crust. In: Holland, H. & Turekian, K. (eds), Treatise on Geochemistry vol. 3, 1–64. Oxford: Elsevier-Pergamon.

Sisson, T.W. 1991: Pyroxene-High Silica Rhyolite Trace-Element Partition-Coefficients Measured by Ion Microprobe. Geochimica et Cosmochimica Acta 55, 1575–1585. doi: Doi 10.1016/0016-7037(91)90129-S

Sparks, R.S.J., Huppert, H.E. & Turner, J.S. 1984: The fluid dynamics of evolving magma chambers. Philosophical Transactions of the Royal Society of London A310, 511–534.

Sun, S.-S. & McDonough, W.F. 1989: Chemical and isotopic systematics of oceanic basalts: implications for mantle composition and processes. In: Saunders, A.D. & Norry, M.J. (eds), Magmatism in the Ocean Basins. Geological Society Special Publication 42, 313–345.

Tegner, C., Lesher, C.E., Larsen, L.M. & Watt, W.S. 1998: Evidence from the rare-earth-element record of mantle melting for cooling of the Tertiary Iceland plume. Nature 395, 591–594.

Tegner, C., Brooks, C.K., Duncan, R.A., Heister, L.E. & Bernstein, S. 2008: ^{40}Ar-^{39}Ar ages of intrusions in East Greenland: Rift-to-drift transition over the Iceland hotspot. Lithos 101, 480–500.

Thórarinsson, S.B., Holm, P.M., Tappe, S., Heaman, L.M. & Prægel, N.-O. 2016: U–Pb geochronology of the Eocene Kærven intrusive complex, East Greenland: constraints on the Ice-

land hotspot track during the rift-to-drift transition. Geological Magazine 153, 128–142. doi: 10.1017/S0016756815000448
Wager, L.R. & Brown, G.M. 1968: Layered igneous rocks. Edinburgh: Oliver & Boyd.
Wager, L.R., Brown, G.M. & Wadsworth, W.J. 1960: Types of igneous cumulates. Journal of Petrology 1, 73–85.
Wedepohl, K.H. 1995: The composition of the continental crust. Geochimica et Cosmochimica Acta 59, 1217–1232. doi: 10.1016/0016-7037(95)00038-2
White, C.M., Geist, D.J., Frost, C.D. & Verwoerd, W.J. 1989: Petrology of the Vandfaldsdalen Macrodike, Skaergaard Region, East Greenland. Journal of Petrology 30, 271–298.
White, R.S. & McKenzie, D.P. 1989: Magmatism at Rift Zones: The Generation of Volcanic Continental Margins and Flood Basalts. Journal of Geophysical Research 94, 7685–7729.
Willbold, M. & Stracke, A. 2006: Trace element composition of mantle end-members: Implications for recycling of oceanic and upper and lower continental crust. Geochemistry Geophysics Geosystems 7(4), 30 pp. doi: 10.1029/2005GC001005
Zen, E. 1986: Aluminum Enrichment in Silicate Melts by Fractional Crystallization: Some Mineralogical and Petrographic Constraints. Journal of Petrology 27, 1095–1117.